The Investigation of Condensed Phosphates of Alkaline Earth Metals for Use as Biomaterials

by KATIE HORE

A thesis submitted to the University of Birmingham for the degree of

MASTERS BY RESEARCH

School of Chemistry

College of Engineering and Physical Sciences

University of Birmingham

January 2011

Abstract

Biomaterials are non-viable substances formulated to interact with biological systems. An ideal biomaterial will be cytocompatible – it will not cause an adverse response in the body – and will have similar physical properties to the material it is replacing.

Group 2 metal phosphates make good biomaterials as they are chemically similar to bone and teeth. The synthesis and structure of magnesium acid pyrophosphate, $MgH_2P_2O_7$ is reported. Attempts to dope calcium and magnesium acid pyrophosphates with metal cations to alter their physical and biological properties are described.

The properties of a material can be modified by producing a composite. The interactions between a naturally occurring polymer, polyhydroxybutrate and calcium polyphosphate were investigated to see if a composite could be formed. It was found that polyhydroxybutrate decomposed at too low a temperature for a calcium polyphosphate composite to occur.

The small piezoelectric properties of bone may assist the healing of any damage. γ-calcium polyphosphate may exhibit a piezoelectric effect. To measure this aligned crystals are required. γ-calcium polyphosphate was synthesised in magnetic and electric fields in an attempt to produce alignment. Although it was found fields did affect the product, it has not so far been possible to quantify or explain this effect.

Acknowledgements

I would like to thank my supervisor, Dr. Adrian Wright for his help and support throughout the research and writing up of my MRes project.

I would also like to thank the Wright group, Dr. Fiona Coomer, Matthew Cave, Thomas Marsh, Colin Slater and Yasmin Begum for their help and practical idea and advice.

Thank you to the Wright group and everyone on Floor 5 for their help and support and making it an enjoyable place to study.

Index

Chapter 1 Introduction

This thesis reports compounds, which may have applications as biomaterials, particularly bone and teeth replacements. Section 1 of the introduction is a brief outline of ideal and current biomaterials. The work in this thesis concentrates on condensed phosphates and therefore, Section 2 is a summary of phosphate chemistry and its relevance to the design of biomaterials. Then, in Section 3 polyhydroxybutrate and calcium polyphosphate composites and their possible application as biomaterials are considered.

1.1 Biomaterials

The replacement of hard tissues in the body, such as bone and teeth, in the event of disease or damage has long been a challenge. The ideal form of transplant is an autologous implant: transplant of bone from a donor site on the patient to the treatment site. This has obvious immune advantages but there are also disadvantages such as few suitable donor sites and increased pain and recovery times for the patient. An alternative is transplanting natural bone tissue from a donor, in the form of allographs (transplants from another human) or xenographs (transplants of non-human tissue). This has many disadvantages including immune responses, rejection of the replacement tissue and the lack of donors. The third type of transplant is artificial biomaterial whose properties can be tuned for their application, and to reduce any possible immune response. Their sterility can be guaranteed and this removes the risk of cross infection.

A biomaterial is a non-viable material which is used in a device intended to interact with

biological systems. The replacement of hard tissues following damage through wear, disease or accident is a large area of biomaterials research. The main requirement of all biomaterials is cytocompatibility, that is, not eliciting an adverse bioresponse. Biomaterials can be completely passive or they can be biocompatible. Biocompatibility is the ability of a material to elicit an appropriate response in the host e.g. a bone replacement material to promote the growth of bone tissue. Factors affecting bioactivity include surface morphology, the presence and size of pores in the material[1] and the chemical composition of the implant. Another important consideration is that any implant ideally needs to have similar physical properties as the material it is replacing or repairing. Moreover, to make an implant commercially viable, it must be easy and cheap to produce in a variety of shapes and easy to sterilise.

The application of biomaterials can be traced back 2000 years, to the Romans using gold in dentistry. In 1880 the first 'modern' biomaterial, ivory, was implanted into patients. In 1902 gold was used to coat prosthetics to increase their cytocompatibility. These implants proved to be a success and led to an increase in the study of materials for use in the body. The metal alloy, Vitallium (cobalt, chromium and molybdenum) was widely used as a biomaterial from about 1938 until the 1960s[2] when potentially harmful corrosion products were recognised. In 1972 Boutin[3] started to develop ceramic biomaterials such as alumina and zirconia. However these materials are not bioactive, and if they are not cemented into place, they can loosen, causing the implant to fail. The bioactive ceramic materials bioglass and hydroxyapatite were developed by Hench[4] and Jarcho respectively in the 1970's.

There are two main classes of ceramic biomaterials currently in use. One is derived from natural sources including coral and coral derivatives or demineralised human or bovine bone.

The second is synthetic ceramics such as bioactive glasses, glass ceramics and calcium phosphates.

Bone and teeth, illustrated in Figures 1 and 2 are made up of both inorganic and organic components. About 65% of bone is inorganic, with the remaining 35% being organic tissue (mainly collagen) and water. The inorganic material is carbonate hydroxyapatite. The organic component of the bone provides most of its elasticity and tensile strength, with the ceramic compounds providing the mechanical strength. There is also evidence that bone is piezoelectric (when a piezoelectric material is subjected to mechanical stress a voltage develops across it) and it had been suggested that this effect may promote the growth of new bone[5]. The composition of teeth is similar to that of bone, but with different proportions of organic and inorganic material.

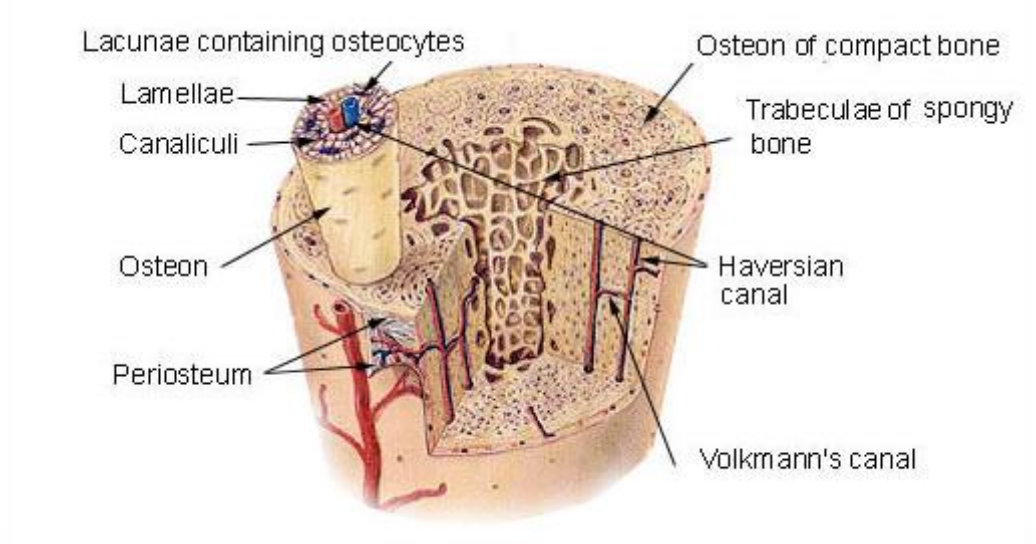

Figure 1: Cross section of a bone (taken from 6).

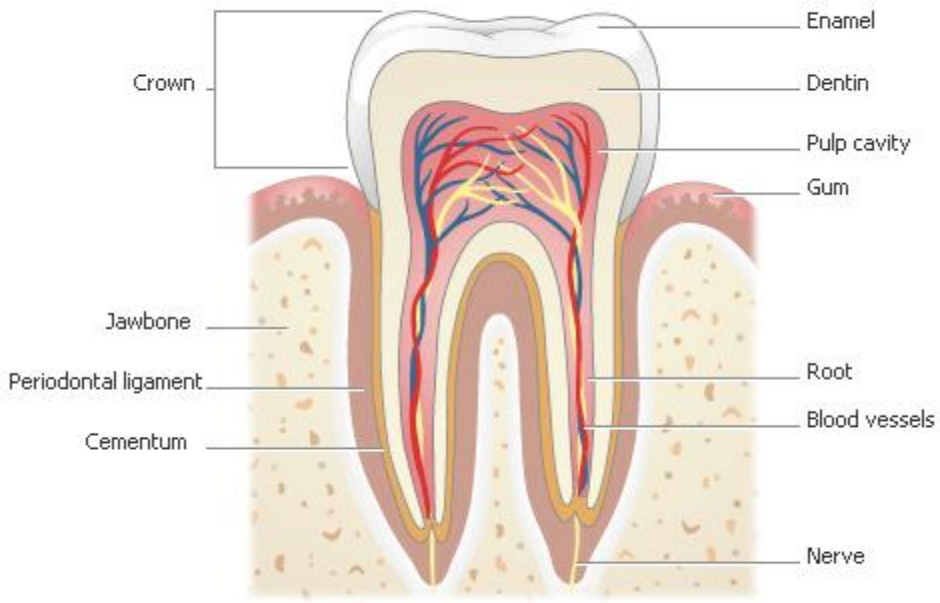

Figure 2: Cross section of a tooth (taken from 7).

The closest synthetic material to the ceramic component of hard tissue is hydroxyapatite $Ca_{10}(PO_4)_6(OH)_2$. As a result there has been a lot of research into its use as a biomaterial.

Phosphates have great potential to be useful biomaterials. The research in this thesis concentrates on condensed phosphate phases. Some of these phases and their properties are summarised below.

1.2 Phosphates

Phosphates are salts of monophosphoric acid, H_3PO_4, and its condensed or polymeric forms. Phosphate ions consist of a phosphorus atom surrounded by an approximately regular

tetrahedron of four covalently bonded oxygen atoms.

1.2.1 Types of Phosphates

The most important and widely studied group of phosphates are the monophosphates (or orthophosphates) which are derived directly from monophosphoric acid. In the many examples of materials containing the phosphate ion the coordination is usually close to a perfect tetrahedron.

By contrast, condensed phosphates are any phosphates which have an oxygen/phosphorus ratio between 5/2 and 4. In these species, PO_4 tetrahedra share one or more of the oxygen ions at their corners. There are many ways the O – P – O bond characteristic of condensed phosphates can form, but the most simple is condensation with the elimination of water, illustrated in Figure 3.

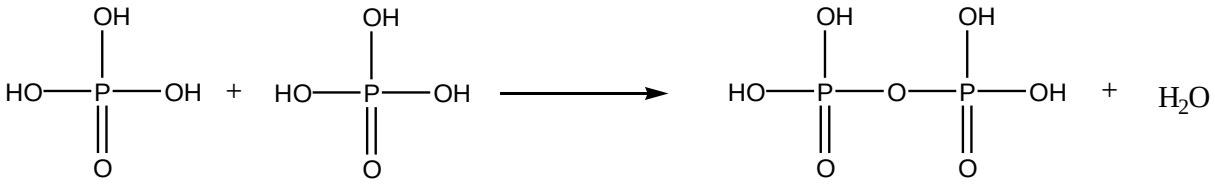

Figure 3: Schematic of the condensation of phosphoric acid.

There are three main forms of condensed phosphates; polyphosphates, cyclophosphate and ultra phosphates illustrated in Figure 4. Polyphosphates is the term used to describe linear chains of the phosphate tetrahedra that share two of their corners. Internal phosphate tetrahedra lie within the chain and share two of their oxygen atoms. Terminal tetrahedra occur

at the ends of the chains and only share one oxygen. The general formula for a polyphosphate is

$$(P_nO_{3n+1})^{(n+2)-}$$

where n is the number of tetrahedra. The oxygen/phosphorous ratio approaches 3 as the number of tetrahedra becomes very large.

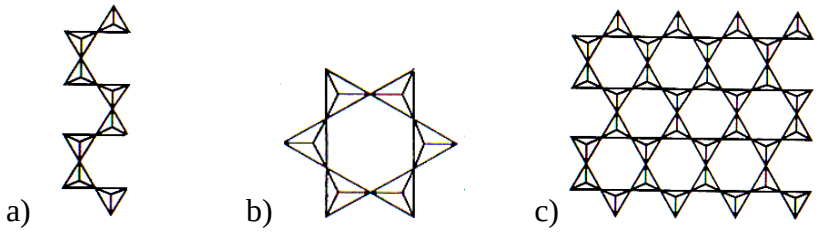

Figure 4: Types of condensed phosphate structure, a) polyphosphate, b) cyclohexaphosphate and c) ultraphosphates

There has been much confusion in the naming of condensed phosphates over the years. Therefore it is helpful to summarise, in Table 1, the nomenclature generally used today.

Table 1: Nomenclature of condensed polyphosphates

Number of tetrahedra	Name
2	Diphosphates or pyrophosphates
3	Triphosphates or tripolyphosphates
4	Tetraphosphates or tetrapolyphosphates
5	Pentaphosphates or pentapolyphosphates
<20	Oligophosphates
Very large or infinite chains	Long chain phosphates or meta phosphates

Cyclophosphates are condensed phosphates where the tetrahedra condense to form cyclic structures with all the ions sharing two oxygen atoms. Rings are known for n = 3, 4, 5, 6, 8, 10 and 12 [8] and they have the general formula $(P_nO_{3n})^{n-}$, for example calcium polyphosphate, $Ca(PO_3)_2$ [9].

Ultraphosphates have tetrahedra which share three oxygen atoms enabling the anion to form various different geometries. These include finite groups, infinite ribbons, infinite layers or three-dimensional networks, for example CaP_4O_{11} [10].

1.2.2 History of the Condensed Phosphates

The first condensed phosphate was reported by Berzelius in 1816[11] when he observed changes when phosphoric acid was ignited. He also prepared condensed phosphates by heating Na_2HPO_4. In 1847 Maddrell prepared and characterised a series of $M(PO_3)_3$ compounds,

where M = Mg, Ni, Co, Cu, Mn, Ca, Sr and Ba, and compounds with trivalent cations, $Cr(PO_3)_3$ and $Al(PO_3)_3$. The progress of discovering new condensed phosphates continued steadily throughout the 19th century but was hampered by the available techniques and the confusion in the nomenclature.

The study of phosphates took off in the 1950's due to the advance of analytical techniques including thin-layer chromatography, used to determine the degree of polymerisation, and X-ray structural analysis. The first condensed phosphate to be structurally characterised was $Zr_2P_2O_7$ [12].

1.2.3 Naturally Occurring Phosphates

Phosphates are found in all types of cells. Their main function is in phosphorylation where a phosphate group is added to organic molecules such as proteins. Phosphorylation and dephosphorylation are used as an on/off switch for many enzymes and receptors, because the presence of a phosphate group can change the conformation of the protein. Phosphates are also used as a buffer by animal cells.

In 1890 Liberman discovered polyphosphate in yeast, and since then long-chain polyphosphates and triphosphates have been identified in all living organisms. The role of triphosphates and the enzymes involved in the metabolic pathway have been extensively studied[13]. However, the relevance of polyphosphates is much less clear and, until recently, they were thought to be 'molecular fossils' or an energy and phosphorus source for micro-organisms at times of stress. However, they have recently been identified as having an

important role in programming a cell to survive under stationary conditions[14,15] and have been identified a component of a structure found in cell membranes which is possibly a calcium ion channel.[16]

1.2.4 Using Calcium Phosphates as Biomaterials

The primary ceramic component of bone is related to hydroxyapatite which is surrounded by an organic matrix, mainly composed of collagen. The chemical similarity of calcium phosphates, and the structural similarity of some forms, to hydroxyapatite means that they have been widely studied as biomaterials. Moreover they are inherently cytocompatible; they are hydrolysed *in vivo* forming calcium ions and monophosphates. Various forms of calcium phosphates have been considered as biomaterials, and these have been summarised below.

Hydroxyapatite (HA), $Ca_5(PO_4)_3(OH)$ is a naturally occurring mineral, which has a very flexible structure allowing substitutions by cations and anions such as calcium with sodium, hydroxide with fluoride or chloride ions and either phosphate or hydroxide with carbonate. Due to the variety of possible substitutions HA can be coloured white, brown, yellow or green. HA usually has a simple hexagonal structure but under certain synthetic conditions adopts a monoclinic structure[17]. The main mineral in bone is a modified form of HA and dental enamel and dentin are made of carbonated calcium-deficient HA. An example of substitution in this context is the addition of fluoride to water and toothpaste, which is thought to improve dental health by increasing the strength of the HA. As HA has a similar composition to bone it has considerable potential as a biomaterial with good biocompatability, bioactivity and osteoconductivity[18].

Monocalcium Phosphate Monohydrate or MCPM, $Ca(H_2PO_4)_2.H_2O$ is a widely used precursor for other calcium phosphate phases, especially for formation via the ceramic method. However, it is highly water soluble and therefore its use as a biomaterial is limited.

Tricalcium phosphate (TCP) has two main forms α-TCP and β-TCP which were both reported in 1932 by G. Tromel[19]. The use of TCP as a biomaterial has been widely investigated, but its relatively high level of degradability *in vivo* and brittleness are disadvantages[20]. TCP is often mixed with relatively insoluble synthetic hydroxyapatite to give a biphasic implant material with an intermediate degradation rate.

Brushite, $CaHPO_4.2H_2O$, is a layered calcium phosphate which has been used as a component in calcium phosphate cements. It is more quickly absorbed *in vivo* than apatite-based cements[21] but it does not have the physical characteristics necessary for load-bearing applications[22].

1.2.5 Calcium Polyphosphate

The phase that is particularly highlighted in this thesis is calcium polyphosphate (Ca PolyP). There are two known polymorphs, β- and γ-$Ca(PO_3)_2$. The structures of the two polymorphs are shown in Figure 5. β-Ca PolyP[23,24] has chains of phosphate groups running unidirectionally through the structure. The unit cell is monoclinic and has a space group of $P2_1/c$. γ-Ca PolyP was synthesised and characterised by the Wright group[9, 25]. By contrast, it consists of layers of unidirectional helical polyphosphate chains stacked in alternating

perpendicular directions along the [110] and [−110] directions. It is also monoclinic but has a different space group, Cc. Helical chains are rare in polyphosphate structures but they have been found in $(NaPO_3)_6$ [26] and $CoK(PO_3)_3$ [27]. The crossed arrangement of these chains appears to be unique not only in phosphates but also in other tetrahedral chain structures including silicates.

Ca PolyPs appear ideal for use as biomaterials: they have high levels of biocompatibility and bioactivity[28] and they degrade *in vivo* to produce products that are non-toxic and do not produce an immune response[29]. Ca PolyP is currently used as a bone substitute[30], for bone screws[31], for teeth crowns[32] and as a drug delivery matrix[33,34]. It has been shown Ca PolyP implants can induce bone formation[28,35]. It also has non-biomedical applications, as an alternative to asbestos fibres[36] and in humidity sensors[37].

The non-centrosymmetric space group (monoclinic, Cc) of γ-Ca PolyP means it potentially has piezoelectric properties. Piezoelectric materials generate an electric potential in response to mechanical stress or *vice versa*. If the material is not short-circuited a voltage develops across it. It has been suggested that the piezoelectric properties of bone affect its growth[38]. Therefore, an implant, which is piezoelectric may be advantageous. In Chapter 5 of this thesis the effect of magnetic and electric fields on the growth of γ-Ca PolyP crystals are studied.

Chapter 4 of this thesis details attempts to produce a composite of γ-Ca PolyP and PHB. Therefore in the next section composites of Ca PolyP are introduced and their use as biomaterials is discussed.

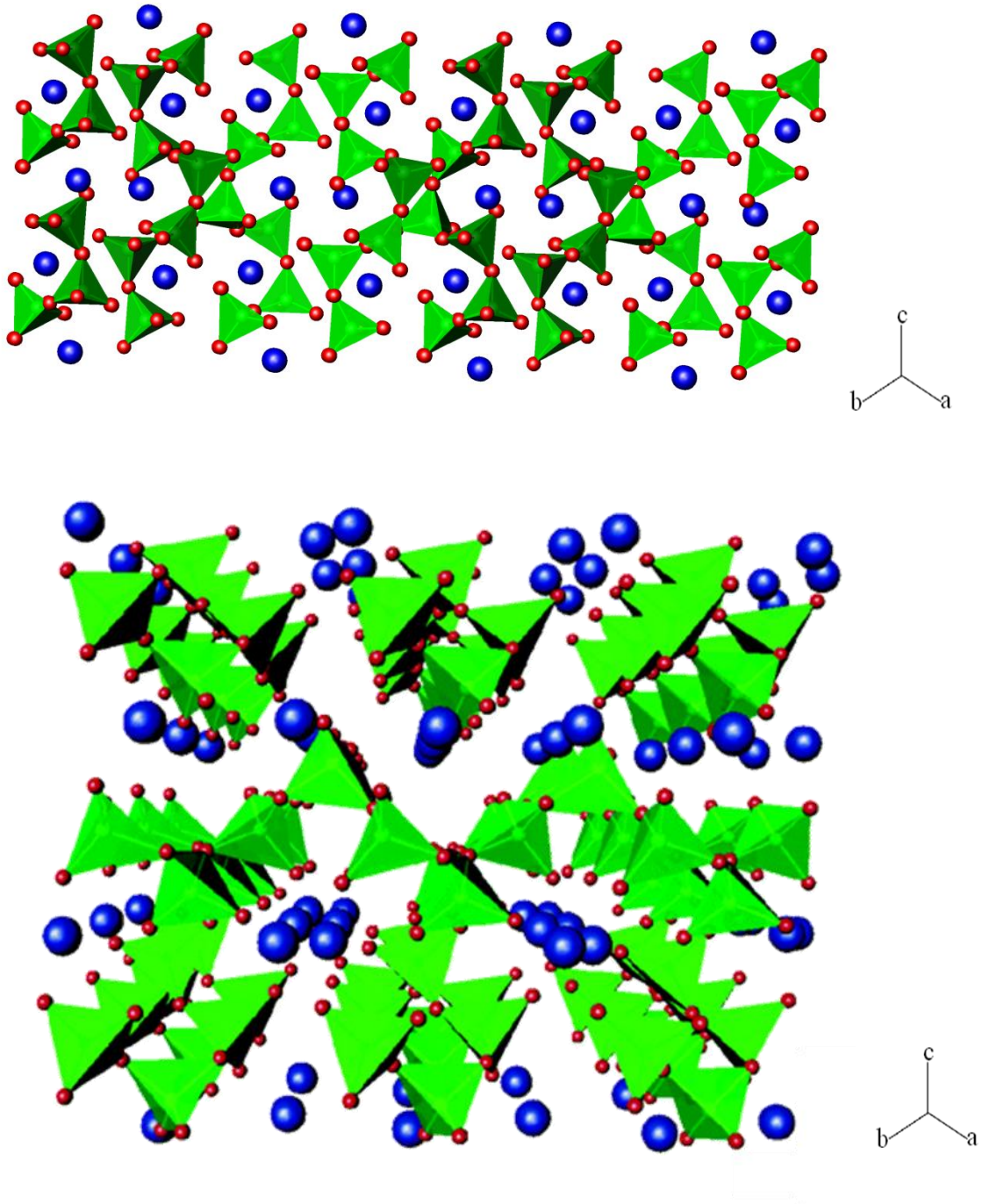

Figure 5: Structures of top: β- and bottom: γ- Ca PolyP. The blue spheres are calcium ions and the green polyhedral are PO_4 tetrahedra.

1.3 Composites of Calcium Phosphates

"[Composite materials] are engineered materials made from two or more constituent materials with significantly different physical or chemical properties"[39]. They allow the physical, biological and mechanical properties of the implant to be tuned to meet specific needs.

There are problems with the use of pure Ca PolyPs as biomaterials including brittleness and lack of strength. Composites can be used to improve the physical properties whilst maintaining or even improving the biological ones. For example, the different components may degrade at different rates allowing bone ingrowth while maintaining a supporting element. Moreover, calcium phosphates and their decomposition products are basic. The breakdown products of many potential biopolymers are acidic and may cause damage to tissues *in vivo*. Therefore, the presence of phosphates in the composite could act as a buffer neutralising any potentially damaging species[40].

Composites of short-chain phosphates such as tricalcium phosphate[41,42] have been widely studied, including porous calcium phosphate networks filled with a polymer such as polycaprolactone[43]. A Ca PolyP composite with a resin has also been made[53]. Here a strong chemical bond is formed between the polyphosphate and the organic polymer resin.

1.3.1 Polyhydroxybutrate

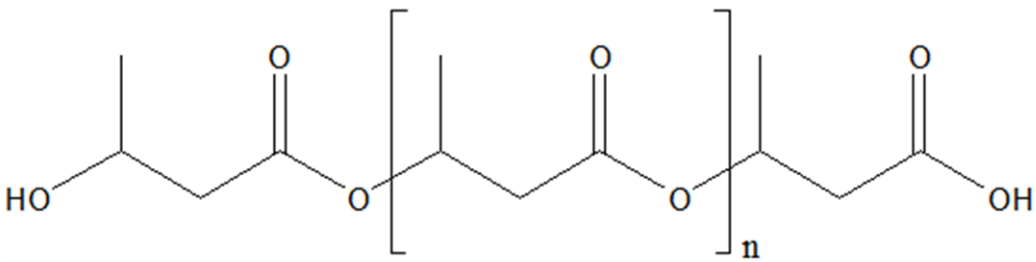

Figure 6: Structure of polyhydroxybutyrate (PHB).

The biological component of the composite considered in this thesis is polyhydroxybutyrate (PHB). The structure of polyhydroxybutyrate (PHB) is shown in Figure 6. PHB is an organic polymer found in every type of living cell. For example, it is used as an energy store in prokaryotic microorganisms under nutrient-limited conditions[44]. It is therefore easily biodegradable and has been used commercially as an environmentally friendly plastic, manufactured by ICI[45]. However it is brittle and the degradation temperature and melting temperature are very close together making processing difficult.

PHB has good cytocompatibility, and short-chain PHB is naturally found in blood and can be easily hydrolysed *in vivo*. PHB has a similar tensile strength to bone, an important factor for fracture repair. Metals currently used as implants are much stronger than bone and can increase the healing time of a fracture and reduce the strength of the new bone formed. However, PHB is not bioactive and bone cannot bond strongly to an implant. Other disadvantages include the poor physical properties detailed above. Many PHB composites have been investigated with the aim of improving its bioactivity, mechanical and processing properties.

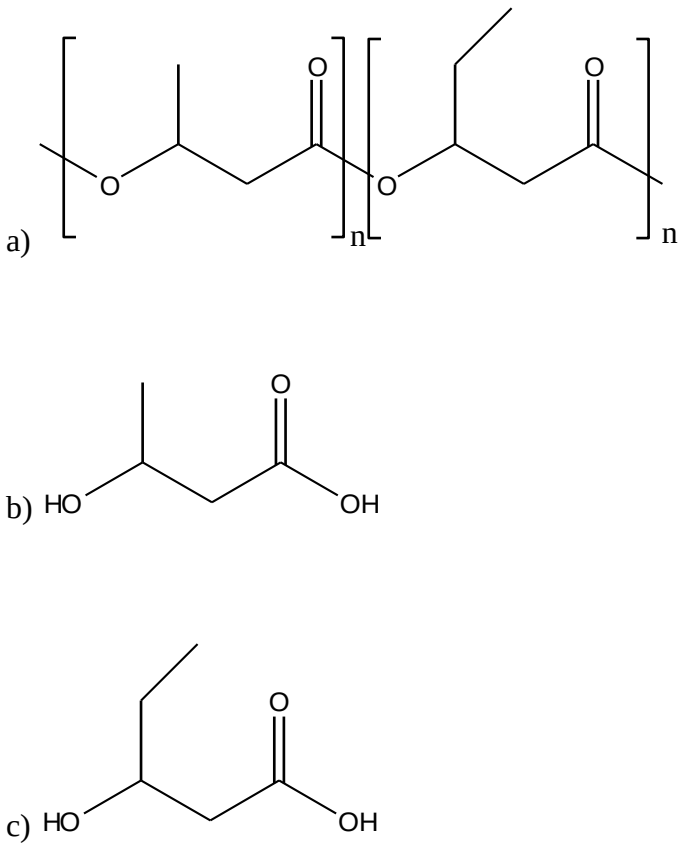

Figure 7: structure of a) PHBV, b) HB monomer and c) HV monomer.

Combining PHB into a composite with materials such as hydroxyapatite (HA)[46,47] and bioglass[48] forms a material with increased strength and bioactivity. Studies on rabbits have shown bone formation on the surface of implants. There have also been studies on the copolymerisation of PHB monomers with similar organic monomers. PHBV, shown in Figure 7 a, is a random copolymer of 3-hydroxybutyrate (HB) and 3-hydroxyvalerate (HV), shown in Figure 7 b and c. Like PHB this compound is found in micro-organisms. It has higher melt stability and better physical properties than PHB. A composite formed of PHBV and wollastonite ($CaSiO_3$)[49], has improved physical properties and bioactivity. The wollastonite acts as a buffer maintaining the local pH as the polymer degrades. PHBV has

also been reinforced using plant fibres[50].

1.3.2 Polyhydroxybutrate and Calcium Polyphosphate Composites

Chapter 4 of this thesis investigates the interactions between PHB and Ca PolyP. This is a promising compound to consider as there is evidence that PHB and Ca PolyP may form complexes in cell membranes[51,52,53]. Based on their properties, and the hydrophobic environment the complex inhabits, two possible structures have been suggested. Reusch et al[51,52] suggested that a Ca PolyP helix is surrounded by PHB coiled in the same conformation it forms in solution. Seebach et al[53] assumed that the PHB surrounded the Ca PolyP is in its solid-state folded helix structure. It has been suggested that this complex may be a calcium ion channel. The suggested helical structure of Ca PolyP in the PHB complex is reminiscent of the phosphate helix that forms in γ-Ca PolyP.

1.3.3 Doping of the Phosphates

Another way to alter the properties of a material is to intentionally introduce impurities into a system. The most widely known use of doping is in the production of semiconductors. In Chapter 4 the doping of an acid pyrophosphate is reported.

Most of the previous studies on doping pure calcium phosphates have been based on glassy calcium phosphates[54], tricalcium phosphates[55] or via mechanical processes such as ball milling[56]. There have also been a lot of studies on the doping of hydroxyapatites[57] as bone and teeth hydroxyapatites contain many trace ions. A strontium-doped Ca PolyP glass has been

shown to have increased growth of cells on its surface and have a lower degradation rate than equivalent undoped phosphates [58, 59].

1.4 Summary of Thesis

In Chapter 2 the experimental and analytical methods used to collect and analyse the data presented in the thesis are detailed. Chapter 3 describes the synthesis and characterisation of a novel phosphate, calcium acid pyrophosphate, $MgH_2P_2O_7$. Structural studies show that this compound has the same structure as $NiH_2P_2O_7$. The doping of $MgH_2P_2O_7$ with calcium and strontium is investigated. As a comparison the doping of magnesium acid pyrophosphate with calcium is also considered.

Chapter 4 describes attempts to produce a composite of calcium phosphate and PHB inspired by cellular phosphate/PHB complexes. Solid state and acid melt synthesis are considered, using both the monomer and the polymer of PHB. The growth of aligned γ-Ca PolyP crystals using magnetic and electric fields is investigated in Chapter 5. Finally Chapter 6 presents a brief summary of the results and details further work that might be done in these research areas.

1.5 References

1 K. J. L. Burg, S. Porter and J. F. Kellam, *Biomaterials*, 2000, **21(23),** 2347-2359

2 X. Seltzer, D. B. Green, R. de la Guardia, J. Maggie and A. Barnett, *Oral Surg.* 1973, **35**, 828 -860

3 P. Boutin and D. Blanquaert, *Revue de Chirurgie Orthopedique et Reparatrice de l'Appareil Moteur*, 1987, **67**, 279-287

4 L. L. Hench , H. F. Paschall, M. Paschall and J Mcvey, *Am. Ceram. Soc. Bull.* 1973, **52**, 432-432

5 F. Jianqing, Y. Huipin and Z. Xingdong, *Biomaterials*, 1997, **18**, 1531-1534

6 http://training.seer.cancer.gov/anatomy/skeletal/tissue.html 15th March 2011

7 http://encarta.msn.com/media_461516411_761559101_-1_1/Structure_of_a_Tooth.html 4th August 2009

8 A. Durif, *Solid State Sci.* 2005, **7**, 760–766

9 L. E. Jackson, B. M. Kariuki, M. E. Smith, J. E. Barralet and A. J. Wright, *Chem. Mater.* 2005, **17**, 4642-4646

10 M. Beucher, *Mater. Res. Bull.* 1969, **4**, 15

11 J. Berzelius, Ann. *Physik*, 1816, **54**, 31-52

12 G. R. Levi and G. Peyronel, *Z. Kristallogr*. 1935, **96**, 481-487

13 J. R. Knowles, *Annu. Rev. Biochem.* 1980, **49,** 877–919.

14 N. N. Rao and A. Kornberg, *J. Bacteriol.* 1996, **178**, 1394-1400

15 A. Kornberg, Inorganic Polyphophates. Biochemistry, Biology, Biotechnology, Progress in Molecular and Subcellular Biology (Special Issue), 1999, 23, Springer-Verlag, Berlin, pp. 1-19

16 I S Kulaev, V M Vagabov and T V Kulakovskaya, The Biochemistry of Inorganic Polyphosphates, 2nd ed. Wiley, 2004 Chapter 4

17 J. C. Elliott, P. E. Mackie and R. A. Young, *Science*, 1973, **180**, 1055-1057

18 W. Suchanek and M. Yoshimura, *J. Mater. Res.* 1998, **13**, 94-117

19 G. Tromel. *Mitt-Kaiser-Wilhelm-Inst Eisenforschg*, 1932, **14**, 25

20 G. Linghong, L. Huui, X. Gao, *J. of Mat. Sci.* 2004, **39**, 7041 – 7047

21 J. Lemaitre, A. Mirtchi and A. Mortier, *Silcates Industrie*, 1987, **10**, 141

22 M. Bohner, U. Gbureck and J. Barralet, *Biomaterials*, 2005, **26**, 6423-6429

23 M. Schneider and K. H. Jost, *Z. Anorg. Allg. Chem.* 1985, **527**, 99-104

24 W. Rothammel, H. Burzlaff and R. Specht, *Acta Crystallogr. Sect. C-Cryst. Struct. Commun.* 1989, **45**, 551-553

25 L. E. Webb, PhD Thesis, University of Birmingham, 2007

26 K. H. Jost, *Acta Crystallogr.* 1961, **14(8)**, 844

27 A. Durif, J.C. Grenier, M. T. Pouchot and D. Tranqui, *Bull. Soc. Fr. Mineral. Crystallogr.* 1966, **89**, 273

28 M.D. Grynpasa, R.M. Pilliara, R.A. Kandela, R.Renlund, M.Filiaggi and M.Dumitriu, *Biomaterials*, 2002, **23**, 2063–2070

29 N. L. Porter, R. M. Pilliar, M. D. Grynpas, *J. of Biomat. Mater. Res.* 2001, **56**, 504-515

30 R. M. Pilliar, M. J. Filiaggi, J. D. Wells, M. D. Grynpas, R. A. Kandel, *Biomaterials*, 2001, **22**, 963-972

31 J . W. Barlow, G. Lee, R. H. Crawford, J . J . Beaman, H. L. Marcus and R. J . Lagow, US Patent, US 6183515B, Feb. 6, 2001.

32 J . W. Barlow, G. Lee, R. H. Crawford, J . J . Beaman, H. L. Marcus and R. J . Lagow, U.S. Patent No. 5,639,402, June 17, 1997.

33 A. Dion, M. Langman, G. Hall and M. Filiaggi, *Biomaterials*, 2005, **26**, 7276–7285

34 S.C. Schofield, B. Berno, M. Langman1, G. Hall, and M.J. Filiaggi1, *J. Dent. Res.* 2006, **85(7)**, 643-647

35 H. Yuan, Z. Yang, Y. Li, X. Zhang, J. D. De Bruijn and K. De Groot, *J. Mater. Sci. Mater. Med.* 1998, **9**, 723–726.

36 E. J. Griffith, *Chemtech*, 1992, **22**, 220-226

37 M. Greenblatt and I Shuk, *Solid State Ionics*, 1996, **86-88**, 995-1000

38 F. Jianqing, Y. Huipin and Z. Xingdong, *Biomaterials*, 1997, **18**, 1531-1534

39 http://en.wikipedia.org/wiki/Composite_materials 24th June 2009

40 W. Linhart, W. Lehmann, M. Siedler, F. Peters, A. F. Schilling, K. Schwarz, M. Amling, J. M. Rueger and M.Epple, *J. Mater. Sci.* 2006, **41**, 4806-4813

41 J. Li, S. Forberg and L. Hermansson, *Biomaterials*, 197, **12**, 438

42 C.-H. Yao, J.-S. Sun, F.-H. Lin, C.-J. Liao and C.-W. Huang, *Mater. Chem. Phys.* 1996, **45**, 6-14

43 L. Yang, J. Wang, J. Hong, J. P. Santerre and R. M. Pilliar, *J. Biomed. Mater. Res. Part A*, 2003, **66A**, 622-632

44 Y. Doi. *Microbial Polyesters*; VCH: New York, 1990.

45 P. A. Holmes, *Phys Techno1*, 1985, **16**, 32-36

46 Y. Liu and M. Wang, *Curr. Appl. Phys*. 2007, **7**, 547-554

47 C. Doyle, E. T.Tanner and W. Bonfield, *Biomaterials* 1997, **72**, 841-847

48 S. K. Misra, S. N. Nazhat, S. P. Valappil, M. Moshrefi-Torbati, R. J. K. Wood, I. Roy and A. R. Boccaccini. *Biomacromolecules*, 2007, **8(7),** 2112-2119

49 H. Li, J. Chang, *Polym. Degrad. Stab*. 2005, **87**, 301-307

50 M. Shibata, K. Takachiyo K. Ozawa, R. Yosomiya and H. TakeIshi, *J. of Appl. Polym Sci.* 2002, **85**, 129–138

51 R. N. Reusch, R. Huang, and L. L. Bramblet, *Biophys. J*. 1995, **69**, 754-766

52 R. N. Reusch and H. L. Sadoff, *Proc. Nat. Acad. Sci. USA*, 1988, **85**, 4176-4180

53 D. Seebach, H. M. Burger, H.-M. Miiller, U. D. Lengweiler and A. K. Beck, *Helv. Chim. Acta*, 1994, **77**, 1099-1123

54 K. Qiu , X. J. Zhao, C. X. Wan, C. S. Zhao, Y. W. Chen, *Biomaterials*, 2006, **27**, 1277–1286

55 W. Xue, K. Dahlquist, A. Banerjee, A. Bandyopadhyay, S. Bose, *J Mater Sci: Mater Med*, 2008, 1**9**, 2669–2677

56 C. C. Silva, M. P. F. Graça, M. A. Valente and A. S. B. Sombra, *Phys. Scr.* 2009, **79**, 1-6

57 N. C. Koseoglu, A. Buyukaksoy, M. H. Aslan and A. Y. *Oral, J. Mater. Sci. Technol.* 2009, **25**, 799-804

58 Y. W. Chen, G. Q. Shi, Y. L. Ding, X. X. Yu, X. H. Zhang, C. S. Zhao, C. X. Wan, *J Mater Sci: Mater Med*, 2008, **19**, 2655–2662

59 Y.W. Chen, T. Feng, G.Q. Shi, Y.L. Ding, X.X. Yu, X.H. Zhang, Z.B. Zhang, C.X. Wan, *Appl. Surf. Sci.* 2008, **255**, 331–335

Chapter 2 Methods

The first section of this chapter describes the synthetic methods used to produce the samples studied in the thesis. Then, in the rest of the chapter, the analytical techniques used to study them are introduced. These include thermogravimetric analysis, X-ray diffraction and Rietveld analysis.

2.1 Synthesis of Condensed Phosphates

2.1.1 Precursor Route: Decomposition of MCPM

To make the composites described in Chapter 4, 1 g of monocalcium phosphate monohydrate MCPM was ground, placed in an alumina crucible and heated in an oven at a temperature between 150ºC and 250ºC for between 1 and 12 h. Polyhydroxybutyrate (PHB) or hydroxybutyrate (HB) were added to some of the samples.

In Chapter 5 work on the alignment of crystals of γ-Ca PolyP is described. To make γ-Ca PolyP pellets, about 0.15 g of precursor MCPM was pressed into a pellet and then heated. A slower heating rate was used to prevent fast water loss, which could have caused the surface of the pellet to become uneven; and to allow time for γ-Ca PolyP crystallites to form. The pellets were heated on a ceramic piezoelectric, an AlNiCo or SmCo magnet, or an alumina surface.

2.1.2 Acid Melt Synthesis

An acid melt synthesis was used to make various polyphosphates including calcium and magnesium phosphates. A source of cations (e.g. $CaCO_3$) were mixed with excess phosphoric acid using phosphorus:cation ratios of between 2:1 and 6:1. The samples were heated for between 12 and 24 hours at temperatures between 180°C and 350°C. The resulting products were washed with distilled water to remove any unreacted phosphoric acid and dried in an oven at about 40°C for 3 h. To make doped calcium phosphate samples, magnesium or strontium ions were added at the beginning of the synthesis.

2.2 Thermogravimetric Analysis

During thermogravimetric analysis (TGA) the changes in the physical and chemical properties of a sample are measured as a function of temperature. Samples are placed in an alumina crucible, and the change in mass is monitored while the samples are heated in the desired atmosphere. A differential thermal analyser (DTA) monitors the energy changes of the sample compared to those of an inert reference. The instrument used in these studies was a Netsch STA 449F1. The technique was used to investigate the behaviour of MCPM upon heating.

2.3 X-Ray Diffraction

X-ray diffraction (XRD) was used to identify the phase (or phases) present in a sample and to assess their purity. It was also used to determine the degree of crystal alignment in a sample.

There are two types of XRD: X-ray powder diffraction (XRPD) and single crystal X-ray diffraction (SCXRD). The experiments in this thesis produced microcrystalline powders and therefore X-ray powder diffraction was employed.

X-rays are produced by firing electrons at a metal target, usually copper. The electrons cause an inner shell electron to be ejected from a metal atom and, when an outer shell electron fills the resulting hole, the energy it loses is emitted as a photon of electromagnetic radiation. There are several possible electrons, which can fill the hole that is formed and so a spectrum will be a set of peaks which are characteristic of the target metal used.

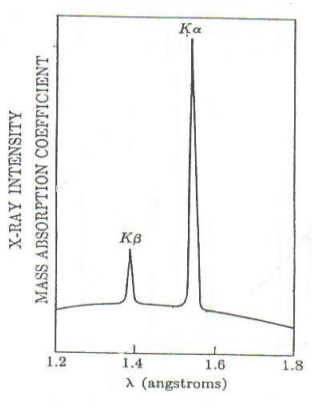

Figure 8: K_α and K_β emission lines for copper.

When copper is used, an electron is ejected from the 1s shell. It is replaced by an electron from the 2p or 3p shells producing the K_α = 1.5418Å and K_β = 1.3922Å lines respectively. The K_α line is actually a doublet as the two electrons in the 2p orbital have different spins and so the energy of their transition to the lower orbital is slightly different. In this work, the diffractometers were fitted with primary beam monochromators, made of germanium, which removed all but one component of the doublet, the $K_{\alpha 1}$ line. The remaining X-rays were then

directed towards the sample and scattered by the electron density in the sample.

An intuitive way to understand X-ray diffraction is using Bragg's model. In a crystal lattice there are sets of parallel planes, which can be identified using Miller indices (*h*, *k*, *l*,). X-rays are reflected off each set of planes, and the reflections interfere constructively when the Bragg equation, illustrated in Figure 9, is satisfied.

$$n\lambda = 2d_{hkl}sin\theta \quad (1)$$

In equation 1, n is an integer, λ is the wavelength of the X-rays, d_{hkl} is the spacing between the planes and θ is the scattering angle.

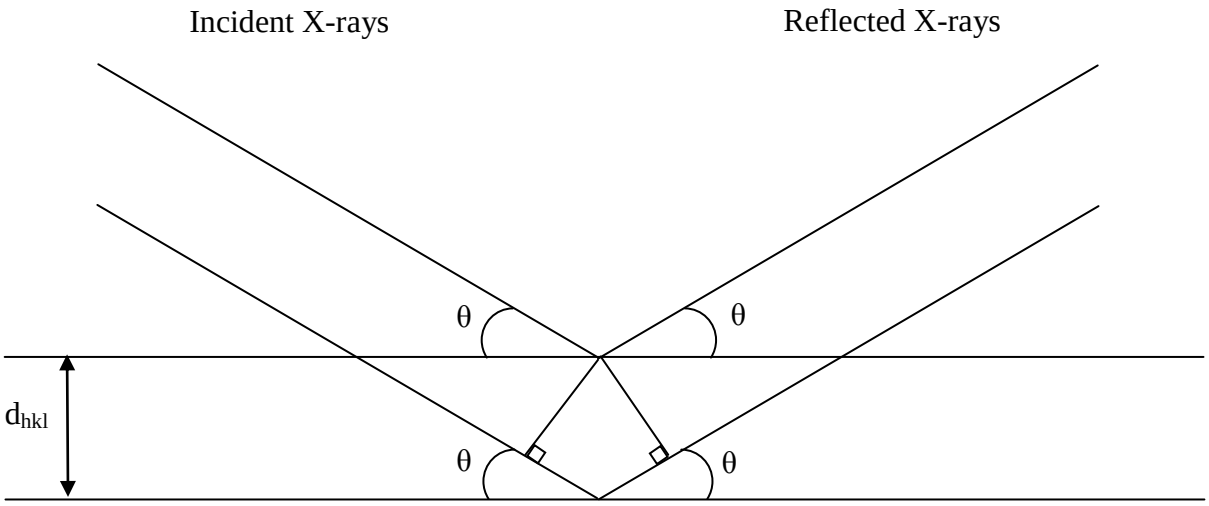

Figure 9: A graphical demonstration of Bragg's Law.

In an ideal powder sample there will be a random orientation of crystals, and therefore X-rays will be diffracted in all the possible directions allowed by Bragg's Law. This gives cones of

reflected X-rays which are projected from the sample as rings of intensity. Each peak in a diffraction pattern represents one of these rings.

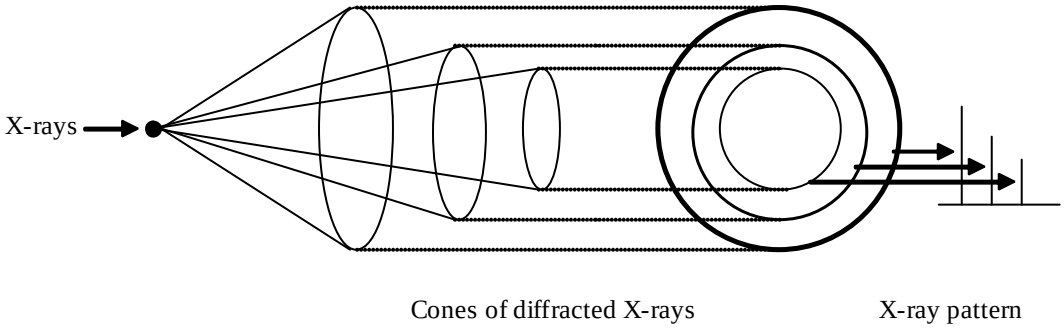

Figure 10: Schematic of X-ray diffraction cones and how the X-ray pattern is generated.

There are two main attributes of XRPD patterns, the intensity of the peaks and the peak positions. The positions of the peaks in the diffraction pattern are determined by the size and the symmetry of the unit cell. The intensity I_{hkl} is a consequence of the relative positions of the atoms within the unit cell and can be calculated as

$$I_{hkl} = Kf_{hkl}^{2}mLpA \qquad (2)$$

where K is a scale factor, f_{hkl} is the structure factor, m is a multiplicity factor, Lp is the Lorentz-polarisation factor and A is an absorption factor.

The structure factor relates the atomic arrangement in the unit cell to the diffraction intensity. The multiplicity factor is the number of equivalent reflections, which lead to one powder line. The Lorentz-polarisation factor is a combination of the Lorentz factor, which is a geometric term that depends on the type of instrument used, and the polarization factor, which accounts

for the polarisation of the beam. The absorption factor takes account of the reduction in the beam intensity due to the absorption of X-rays; this is more of a problem when using transmission mode or when the sample contains heavy atoms which often have a high absorption factor.

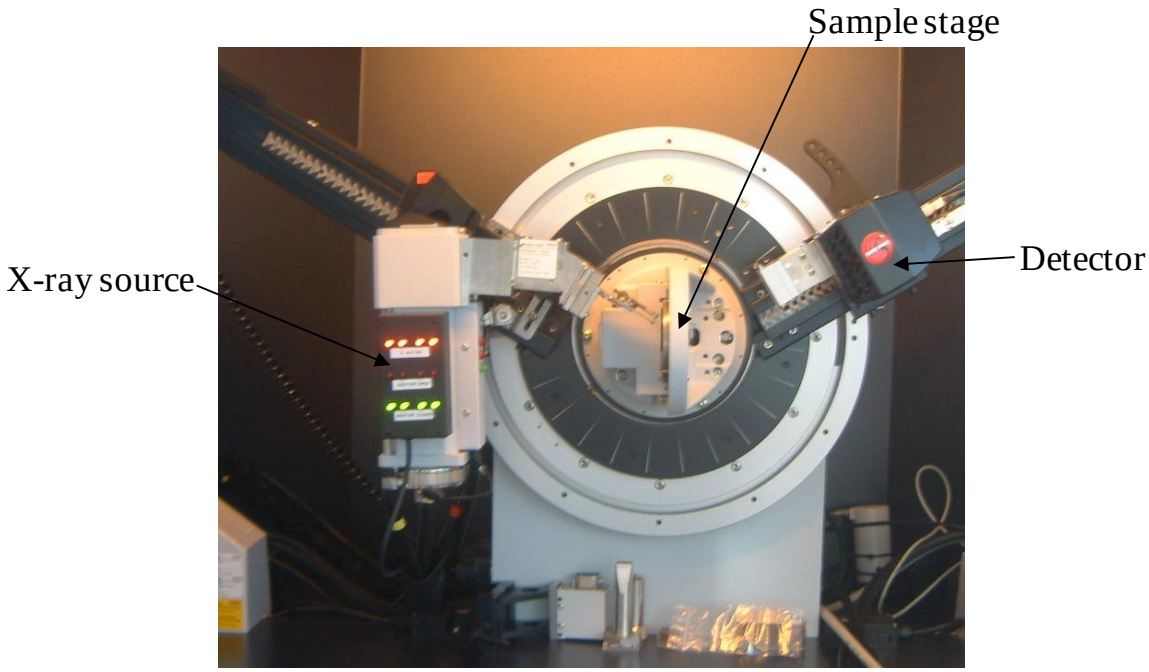

Figure 11: D8 diffractometer in transmission mode.

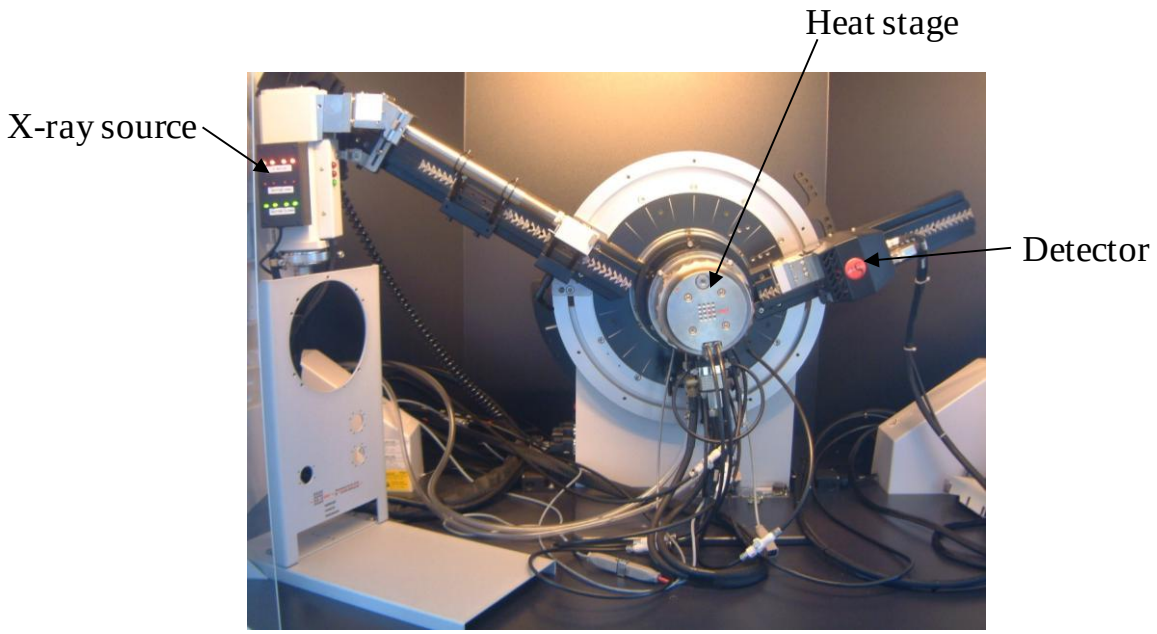

Figure 12: D8 diffractometer in reflection mode with the heat stage fitted.

The majority of measurements were made on a Siemens D8 diffractometer in transmission mode with a samples changer, pictured in Figure 11. Transmission diffractometry has advantages over reflection diffractometry when taking measurements of samples which contain lower molecular weight atoms such as those described in this thesis. In transmission mode the X-rays will pass through the whole sample allowing for maximum possible scattering. By contrast, in reflection mode the X-rays are only scattered from the top few micrometers of the sample.

The alignment of crystallites in γ-Ca PolyP samples, described in Chapter 5, were investigated using a Siemens D8 diffractometer in reflection mode without spinning, pictured in Figure 12. Reflection mode was used on the pellets because the limited penetration of X-rays through them in transmission mode. The samples were not spun to aid identification of any preferred orientation.

The heat stage on the reflection D8 was also used to determine the sequence of phases formed in the decomposition of MCPM to form γ-calcium polyphosphate (Ca PolyP), research described in Chapter 4.

The identification of the phases was performed by comparison to reported XRD patterns using a peak search package, JCPDS (Joint Committee on Powder Diffraction Standards)[1]. Chekcell[2], a program to refine unit cell parameters and volume via a least squares refinement, was also used. More detailed analysis was done in the GSAS (General Structure Analysis System)[3] via Rietveld refinements, as described in the next section.

2.4 Rietveld Analysis

Rietveld analysis is a method, first described in 1967[4], for the characterisation of crystalline materials using neutron or X-ray diffraction data from powder samples. Least squares refinement is used to obtain the best match possible between a pattern calculated from a model and the experimental results. The calculated pattern is based on a crystal structure (or structures), optics effects, machine parameters and other factors including lattice and thermal parameters[5]. During the refinement the calculated parameters are fed back into the system after each cycle improving the model structure until convergence is reached. The quantity that is being minimised in the least squares fit is the residual S_y which can be defined as

$$S_y = \sum_i \omega_i (y(obs)_i - y(calc)_i)^2 \quad (3)$$

where $\omega_i = 1/y(obs)_i$, $y(obs)_i$ is the observed intensity at the *i*th step and $y(calc)_i$ is the calculated intensity at the *i*th step.

The progress of the refinement is judged by visual inspection of a plot showing the difference between the experimental and the calculated patterns, and the feasibility of the resultant structure is monitored. Statistical measures (R_{wp}, R_p, χ) are also used. R_{wp}, the weighted pattern R factor, defined by

$$\frac{\{\sum_i \omega_i [y(obs)_i - y(calc)_i]^2\}^{\frac{1}{2}}}{\{\sum_i \omega_i y(obs)_i{}^2\}^{\frac{1}{2}}} \quad (4)$$

is the best measure to show the progression of the refinement. R_p, the profile *R* factor, is based on the difference between the observed and calculated intensity values, *y*(obs) and *y*(calc)

$$R_p = \frac{\sum_i |y(obs)_i - y(calc)_i|}{\sum_i |y(obs)_i|} \quad (5)$$

χ is the 'goodness of fit' parameter and is another useful indicator of the quality of the refinement. It can be expressed as:

$$\chi = \left[\frac{S_y}{(N-P)}\right]^{\frac{1}{2}} = \frac{R_{wp}}{R_e} \quad (6)$$

where N is the number of observations, P the number of variables and R_e is R-expected

$$R_e = \left[\frac{(N-P)}{\sum \omega_i y(obs)_i{}^2}\right]^{\frac{1}{2}} \quad (7)$$

There are disadvantages to Rietveld analysis. The initial model must be a good approximation to the final structure to allow the least squares refinement to fit the model, and the calculated patterns from a given model will never exactly fit an experimental pattern.

2.5 References

1 JCPDS, *International Centre for Diffraction Data,* 1999

2 J. Laugier and B. Bouchu http://www.ccp14.ac.uk/tutorial/lmgp/index.html#chekcell retrieved December 2009

3 A. C. Larson and R. B. V. Dreele, *General Structure Analysis System,* Los Alamos National Laboratory, 1994

4 H. M Rietveld, *Acta Crystallogr.* 1967, **22**, 151

5 R. A. Young, *The Rietveld Method,* Oxford University Press, New York, 1993

Chapter 3: Magnesium Acid Pyrophosphates

There have been investigations of transition metal phosphates because of their potential use in lithium batteries[1], proton conductors[2] and heterogeneous catalysts[3,4]. In this chapter the structure of magnesium acid pyrophosphate, $MgH_2P_2O_7$ is determined and discussed. Magnesium is of interest given its important role in biological systems and it is present as a component in hard tissue, but little is known of the magnesium condensed acid phosphate systems. Along with biomaterials interest, these solid acid systems may also be useful as ionic conductors or catalysts. In addition, attempts to dope acid pyrophosphates with group II ions are described, and the results are related to the pyrophosphate structures.

3.1 Experimental

3.1.1 Synthesis of $MgH_2P_2O_7$

Attempts to synthesize magnesium acid pyrophosphate, $MgH_2P_2O_7$ were made using acid melt syntheses. Various ratios of P:Mg were attempted but an apparently crystalline single phase was obtained with a ratio of phosphorus to magnesium of 4:1. The optimum synthesis used 0.53 g magnesium oxide, mixed with 6 g phosphoric acid and heated at 180°C for 12 h. The sample was washed with deionised water to remove unreacted phosphoric acid and then dried at 40°C for 3 h.

3.1.2 XRPD Analysis

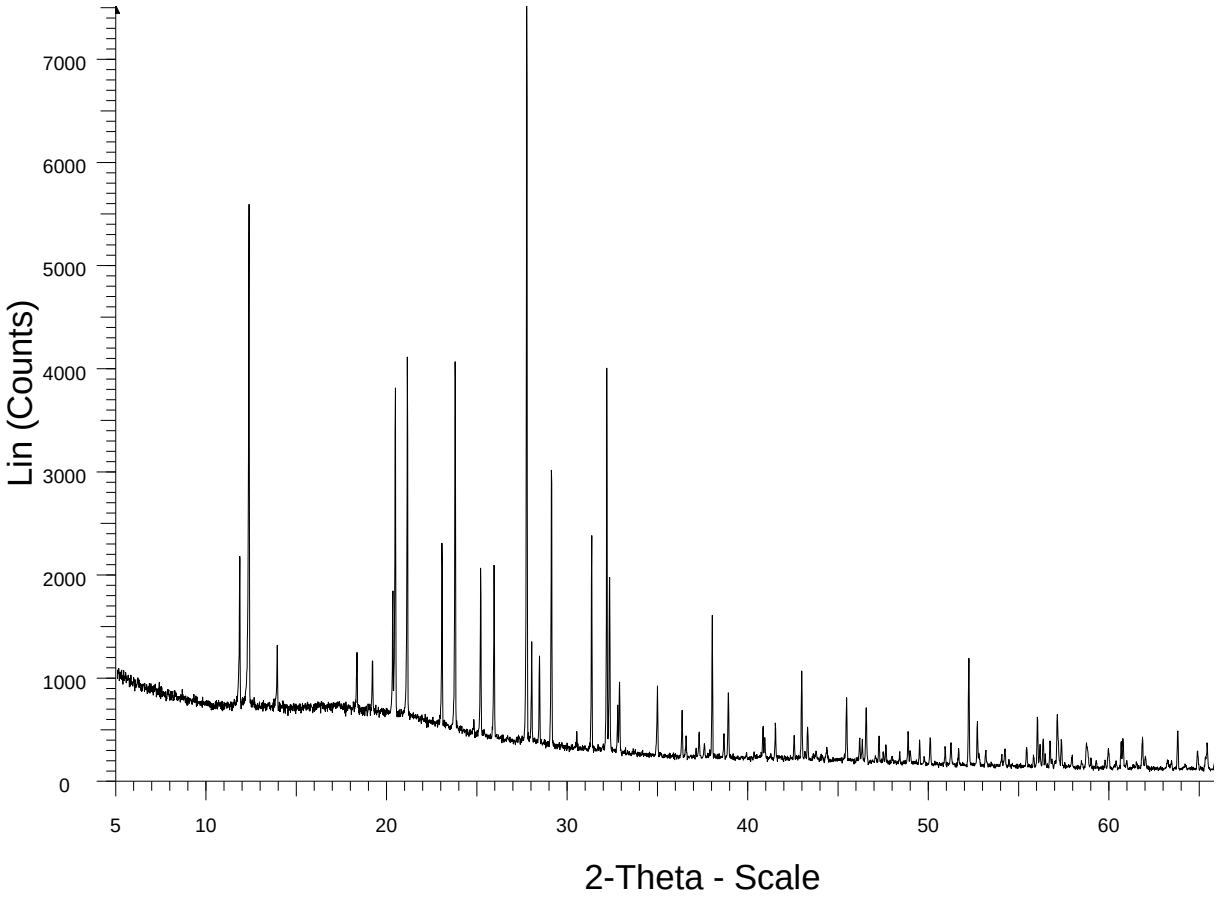

Figure 13: XRD pattern of $MgH_2P_2O_7$.

The X-ray diffraction data from this sample (Figure 13) was analysed and compared using the ICDD JCPDS database to identify the product. No matches were found, even to $CaH_2P_2O_7$[5] and therefore indexing of the pattern was attempted. This involved the accurate measurement of the observed peak positions and these were then entered into the CRYSFIRE indexing program[6]. A possible unit cell was identified and then a search of known structures provided a potential match to $NiH_2P_2O_7$ [7].

3.1.3 Rietveld analysis

The XRPD patterns suggested that the structures of $NiH_2P_2O_7$ and $MgH_2P_2O_7$ are similar and so the $NiH_2P_2O_7$ structure was used as a starting point for a Rietveld analysis. Details of this approach are given in Section 2.4 In the analysis the temperature factors for all oxygen and phosphorus atoms were linked together to aid the stability of the refinement.

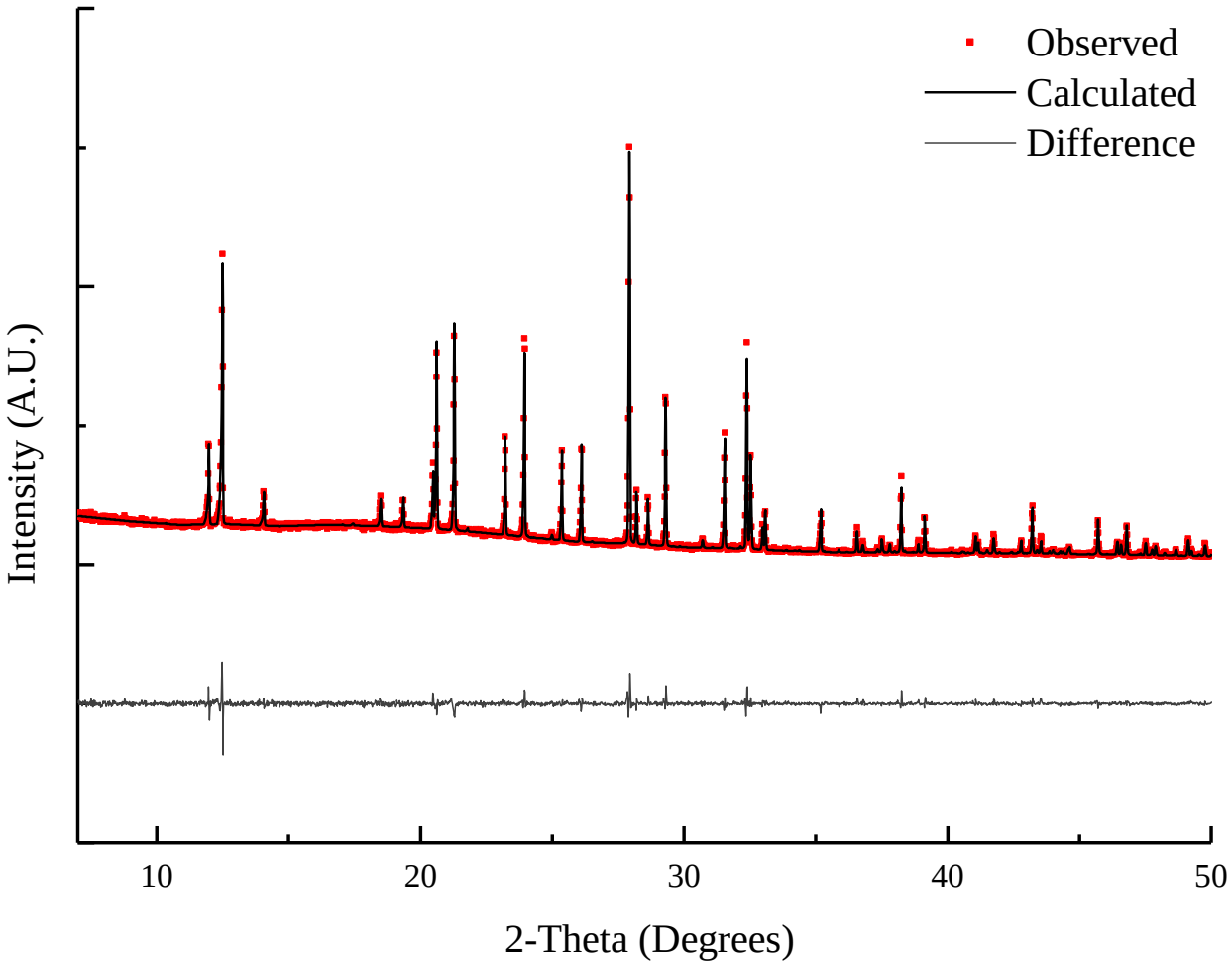

Figure 14: Plot of the Rieveld refinement. Black line is the calculated refinement; the red dots are the experimental pattern and the grey line is the difference between the calculated and the experimental patterns.

Figure 14 is a plot of the refinement used to determine the structures of $MgH_2P_2O_7$. The plot shows the experimental pattern, the pattern calculated from the refinement and the difference between the two. It is a visual representation of the how good the refinement is. The analysis was successful with a χ^2 value of 1.86 and R_{wp} of 6.61%. A summary of the structure is shown in Table 1. Atomic coordinates of the atoms, bond lengths and selected bond angles in a unit cell of $MgH_2P_2O_7$ are listed in Appendix A.

Table 1: Crystallographic data for $MgH_2P_2O_7$

Empirical formula	$MgH_2P_2O_7$
Formula weight	216.04
Crystal system	Monoclinic
Space group	$P2_1/c$
a	9.0209(1) Å
b	12.7095(1) Å
c	9.6083(1) Å
β	106.15(5)°

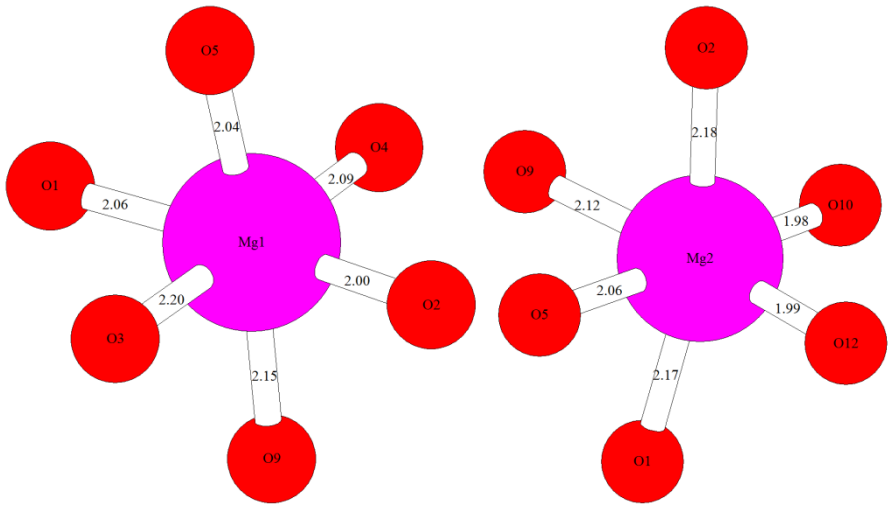

Figure 15: Magnesium octahedra from a unit cell of $MgH_2P_2O_7$ (magnesium in pink and oxygen in red) showing bond lengths.

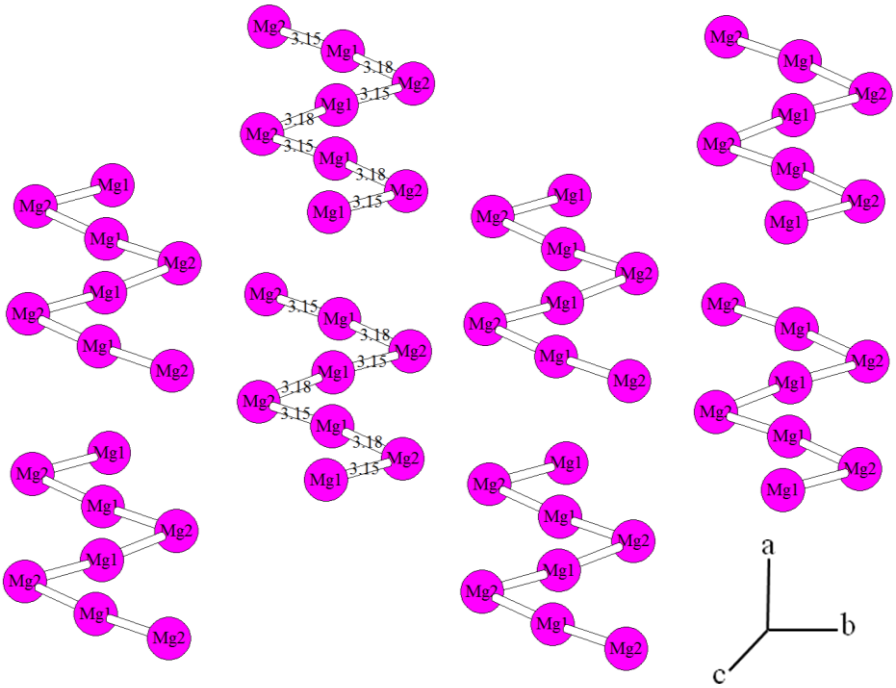

Figure 16: Zigzag magnesium backbone from the $MgH_2P_2O_7$ structure.

The analysis shows that in a unit cell of $MgH_2P_2O_7$ oxygen atoms octahedrally coordinate the magnesium ions as shown in Figure 15. The octahedra share two edges to form a zigzag chain which runs along the *c* axis illustrated in Figure 16. The phosphorus atoms are tetrahedrally coordinated and corner share to form pyrophosphate (P_2O_7) units. The P_2O_7 groups and the Mg octahedra share corners in two types of rings, one with two octahedra and one tetrahedron and the other with one octahedron and two tetrahedra. The structure also has small intersectional 10- and 8- ring channels along the *a* and *c* axis respectively, shown in Figure 17. The bond valence (BV) values for the Mg1 and the Mg2 environments are 2.093 and 2.138 respectively, which is close to the expected values for Mg^{2+} and this supports this structure assignment.

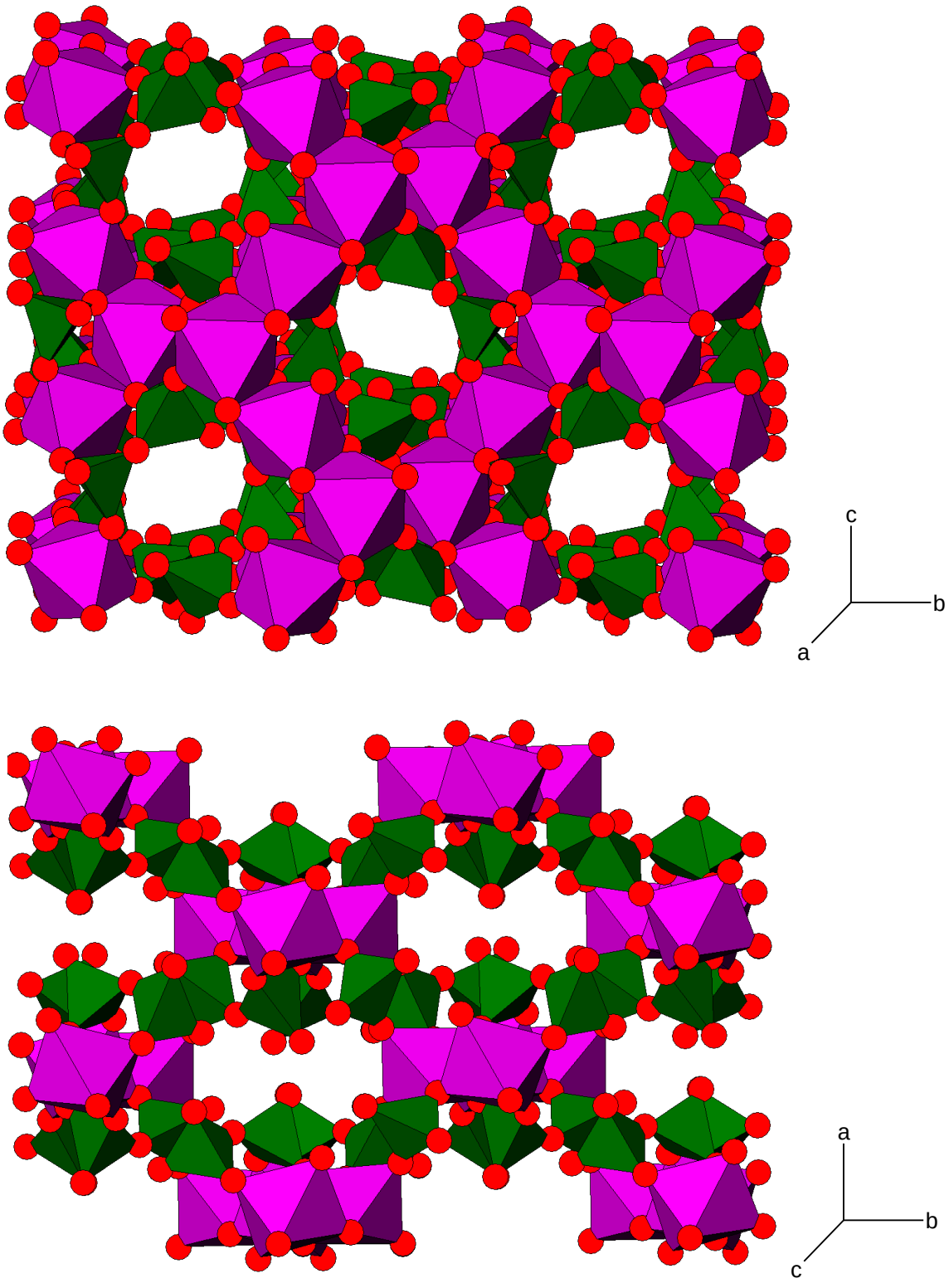

Figure 17: $MgH_2P_2O_7$ projection along the *a* axis (top) and *c* axis (bottom) showing ring channels (MgO_6 in magenta, PO_4 in green).

3.1.4 Comparing the structures of $MgH_2P_2O_7$ and $NiH_2P_2O_7$

The refinement was based on the structure of $NiH_2P_2O_7$. The refined $MgH_2P_2O_7$ structure and the initial $NiH_2P_2O_7$ structure are therefore isostructural, but it is interesting to consider the differences between bond lengths and angles. The Mg–O bond lengths in the magnesium octahedra (see Figure 15) are on average slightly longer than the Ni–O bond lengths, which is to be expected as the Mg^{2+} ion is larger (0.72 Å) than the Ni^{2+} ion (0.69 Å). The P–O bond lengths vary between 1.47 and 1.61 Å in the nickel structure and between 1.44 and 1.70 Å in the magnesium structure. The increased variation in $MgH_2P_2O_7$ is because the refinement used XRPD data rather than a neutron data or structural analysis from SCXRD. Oxygen and phosphorus are both weak X-ray scatterers and so determining their positions with a high degree of accuracy from an X-ray pattern is often difficult. Constraining the phosphorus and oxygen temperature factors will also have affected the positions of the atoms.

The bond angles between adjacent oxygen in the octahedral in the magnesium and nickel structures are very similar, they vary between 77.75° and 99.32° in $MgH_2P_2O_7$ and 78.01° and 99.95° in $NiH_2P_2O_7$.

3.1.5 Hydrogen Atom Positions

The hydrogen positions were not refined as hydrogen atoms are very weak X-ray scatterers and make little contribution to the X-ray pattern. However, the similarities between the nickel and the magnesium structures mean that the hydrogen atoms are likely to be in similar

locations. Therefore the hydrogen positions in the nickel structure, listed in Table 2, were used to give an indication of those in $MgH_2P_2O_7$. Figure 18 shows the phosphorous and oxygen network for $MgH_2P_2O_7$, with the hydrogen atoms at these positions to give an indication of the complete structure.

Many other phosphates have hydrogen atoms which bridge between two oxygen atoms, creating very strong bonds which help to maintain the structure[8]. If the hydrogen atoms are bridging there will be two oxygen atoms which are particularly close together (i.e.2.4-2.6 Å). However there are no unusually short O–O distances in the magnesium structure and this indicates the hydrogen atoms are localised on a single hydrogen and effectively for a hydroxyl group. This is interesting as it suggests that these protons are exchangeable or might be available for proton conductivity or catalysis. Neutron studies on deuterated samples would allow the locations of the hydrogen atoms to be determined more accurately.

Table 2: Hydrogen positions in $NiH_2P_2O_7$ [5]

Atom	*x*	*Y*	*z*	*U*iso × 100
H1	0.4454	-0.0962	0.1701	0.041
H2	0.0253	0.5777	0.3274	0.033
H3	0.6911	0.2473	0.6851	0.057
H4	-0.1399	0.3266	-0.0345	0.030

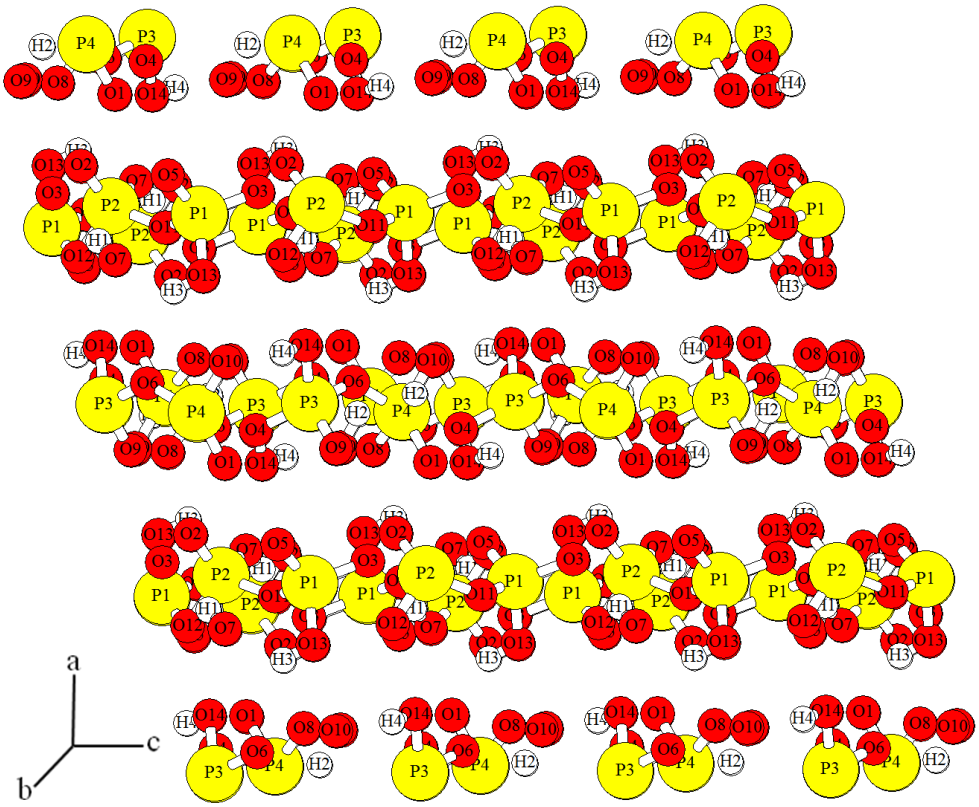

Figure 18: $MgH_2P_2O_7$ with the Mg ions omitted for clarity.

3.1.6 Comparing the Structures of $MgH_2P_2O_7$ and other Condensed Magnsium Phosphates

The structure of magnesium acid pyrophosphate was compared to that of other magnesium phosphates. The magnesium pyrophosphate $Mg_2P_2O_7$ has two polymorphs, α and β. α-$Mg_2P_2O_7$ has two magnesium environments: Mg1 is 5-coordinated and Mg2 is 6-coordinated. β-$Mg_2P_2O_7$ has one magnesium environment, which is octahedrally coordinated. The bond lengths of the octahedrally coordinated magnesium sites are comparable to the octahedrally coordinated Mg sites of $MgH_2P_2O_7$, ranging between 2 and 2.2 Å.

Longer chain phosphates, tetraphosphate, $Mg_2P_4O_{12}$ and polyphosphate, Mg_3PO_4, also have similar Mg bond lengths. The tetraphosphate has two magnesium environments both of which are octahedrally coordinated. The bond lengths are similar to $MgH_2P_2O_7$, although the variation in bond lengths is slightly lower. Mg_3PO_4 has two magnesium environments, one 6-coordinated and the other 5-coordinated. As in $NiH_2P_2O_{7,}$ there is less variation in the phosphorus-oxygen bond lengths in other magnesium phosphates than in $MgH_2P_2O_7$.

The O–Mg–O angles in the $Mg_2P_2O_7$ octahedra are comparable to those in other magnesium phosphates. The bond angles in the $Mg_2P_2O_7$ phosphate tetrahedra are slightly distorted. They vary between 95.16 and 122.68° (compared to the ideal tetrahedral bond angle of 109°) but they are still comparable to the other magnesium phosphates.

3.1.7 Comparing the Structures of $MgH_2P_2O_7$ and $CaH_2P_2O_7$

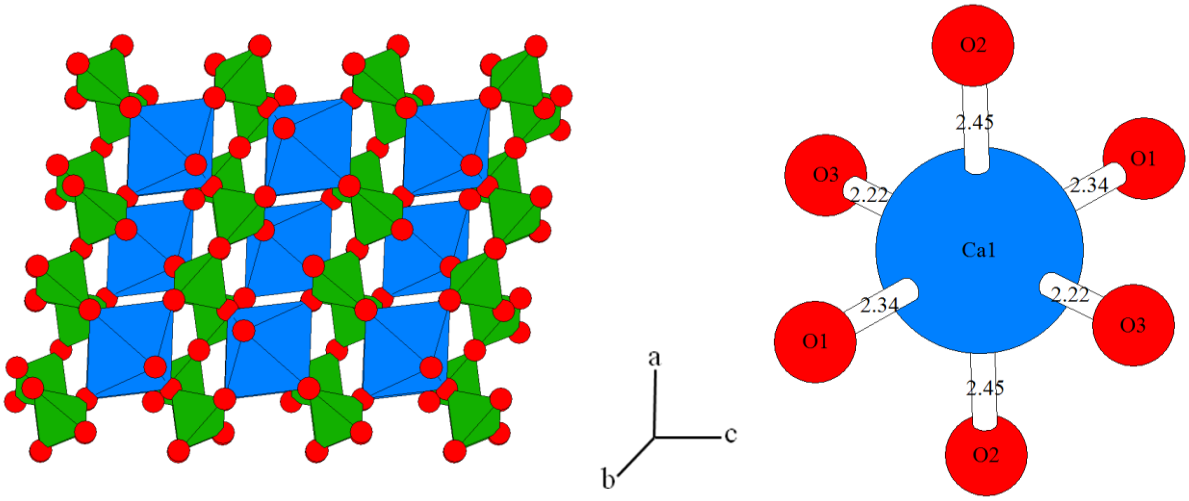

Figure 19: Left: $CaH_2P_2O_7$ structure with CaO_6 octahedra in blue, PO_4 tetrahedra in green and O ions in red. Right: Ca-O polyhedron with the calcium in blue and oxygen in red.

The other well known s-block acid pyrophosphate is $CaH_2P_2O_7$. Its structure is summarised in Table 3 and depicted in Figure 19. Its structure is different to that of the magnesium compound. However, it has similar cation octahedra and pyrophosphate groups. The overall symmetry is higher, with only one cation and one phosphorus environment per unit cell, and the calcium octahedra are linked by corner sharing with the P tetrahedra rather than by the edge sharing tetrahedra in $MgH_2P_2O_7$. The Ca–O bond lengths are, as expected, around 20% larger than the Mg–O bonds in the octahedra, while the P–O bonds in the P tetrahedra are similar in both structures. The cation–O and the P–O bond angles in the octahedra and the tetrahedra respectively are also comparable between the two structures.

Table 3: Summary of the $CaH_2P_2O_7$ structure[9].

Empirical formula	$CaH_2P_2O_7$
Formula weight	216.04
Crystal system	Monoclinic
Space group	C2/c
a	7.3276(1)
b	8.1282(1)
c	9.7632(1)
β	101.2390(7)

3.2 Doping acid pyrophosphates

Cation or anion doping can be an extremely useful tool in changing the physical and chemical properties of a material. Many phosphates have been successfully doped [10,11,12]. Of particular interest in this thesis is any potential change to the bioresponse *in vivo* that may arise from mixtures of cations in potential biomaterials. This study will focus on Ca, Sr and Mg pyrophosphates as these materials have potential as biocompatible materials[13] and also act as precursors to further condensed species (e.g. $CaH_2P_2O_7$ to $Ca(PO_3)_2$ [14]) Attempted doping of $CaH_2P_2O_7$ with magnesium and strontium ions and $MgH_2P_2O_7$ with calcium ions.

3.2.1 Method

The samples were prepared in the same way as other acid melt samples. Different proportions of the main ion source (calcium hydroxide or sodium oxide) were replaced with a source of

the doping ion (calcium hydroxide, strontium carbonate or magnesium oxide) while maintaining a phosphorus : cation ratio of 4:1. The products were analysed using XRPD and the unit cell dimensions were determined using the Chekcell program detailed in Section 2.3.[15]

3.2.2 Results

Table 4 Unit cell dimensions and volumes for doped group 2 acid pyrophosphates.

$CaH_2P_2O_7$ with magnesium ions

Percentage Mg ions	*a* (Å)	*b* (Å)	*c* (Å)	β (°)	Volume (Å^3)
0	7.3234(67)	8.1288(61)	9.7581(82)	101.24(3)	569.75(5)
2	7.3171(14)	8.1154(16)	9.7556(19)	101.24(1)	568.18(1)
5	7.3192(22)	8.1190(27)	9.7559(26)	101.24(1)	568.62(2)
10	7.3190(53)	8.1122(54)	9.7588(70)	101.23(3)	568.31(5)
20	7.3224(31)	8.1193(40)	9.7592(38)	101.24(2)	569.09(3)

$CaH_2P_2O_7$ with strontium ions

Percentage Sr ions	*a* (Å)	*b* (Å)	*c* (Å)	β (°)	Volume (Å^3)
0	7.3208(50)	8.1194(36)	9.7618(52)	101.24(1)	569.12(2)
2	7.3216(29)	8.1206(26)	9.7558(45)	101.24(1)	568.92(2)
5	7.3216(30)	8.1234(29)	9.7585(39)	101.24(2)	569.27(3)
10	7.3221(36)	8.1218(34)	9.7590(43)	101.24(2)	569.22(3)
20	7.3222(33)	8.1216(31)	9.7576(40)	101.24(3)	569.14(3)

$MgH_2P_2O_7$ doped with calcium ions

Percentage Ca ions	*a* (Å)	*b* (Å)	*c* (Å)	β (°)	Volume (Å^3)
0	9.0069(64)	12.6898(79)	9.5972(69)	106.14(3)	1053.66(5)
2	9.0123(42)	12.6950(51)	9.5974(47)	106.15(2)	1054.74(3)
5	9.0070(43)	12.6921(62)	9.5959(49)	106.15(2)	1053.71(4)
10	9.0041(68)	12.6869(86)	9.5932(72)	106.15(3)	1052.65(5)

Table 4 lists the unit cell dimensions and volumes for the doped group 2 acid pyrophosphates. The results do not show conclusive evidence of doping for any of the pyrophosphate structures but there is some indication that the presence of doping ions may be affecting the structures. For $CaH_2P_2O_7$ doped with magnesium ions there a slight decrease in the *a*, *b* and *c* lengths when the doping is at 2%. However from 2-20% there is no significant change. The expected trend when doping with magnesium is a decrease in the unit cell size: Mg^{2+} is smaller than Ca^{2+} and so increasing the amount of Mg^{2+} in the compound would be expected

to decrease the size of the unit cell. The changes are within 3 ESDs and are therefore not significantly different from each other but repeated experiments gave the same trend. This may suggest that a doping level of < 2 % may be possible, but further Mg incorporation is not evident from the plateau in cell volumes as > 2%.

The doping of $CaH_2P_2O_7$ with strontium shows no clear trends, with an increase in the *a*, *b* and *c* parameters expected as Sr^{2+} is larger than Ca^{2+}, 118 and 100 Å respectively.

In addition, there is little obvious trend in the unit cell dimensions for $MgH_2P_2O_7$ doped with calcium. When 20% calcium was used the product was a paste which did not dry and was assumed to be amorphous.

3.2.3 Why were the results inconclusive?

Magnesium, calcium and strontium acid pyrophosphate all have different chemical structures indicating that group two acid pyrophosphates are very dependent on the size of the cation. Any change in the size of the cation will destabilize the structure, so the structure appears very sensitive to doping. The size dependency of the cation sites are confirmed by bond valance (BV) calculations.

Table 5: Bond valence calculations for alternative cations in the cation sites of $MgH_2P_2O_7$ and $CaH_2P_2O_7$.

Structure	Atom	BV
$MgH_2P_2O_7$	Mg1	2.058
$MgH_2P_2O_7$	Mg2	2.066
$MgH_2P_2O_7$	Ca in Mg1 site	4.235
$MgH_2P_2O_7$	Ca in Mg2 site	4.332
$CaH_2P_2O_7$	Ca	2.281
$CaH_2P_2O_7$	Mg in Ca site	1.088
$CaH_2P_2O_7$	Sr in Ca site	3.431

BV calculations indicate the instability of a larger or smaller atom on a given site. Table 5 shows the BV values for calcium in the magnesium structure and magnesium and strontium in the calcium structure. The closer the BV value to the expected charge on the cation, 2+ in all these cases, the more stable it is at that particular site. The values for magnesium and calcium in their own structures are as expected. Ions replacing a smaller ion have larger BV values, e.g. calcium in $MgH_2P_2O_7$ and strontium in $CaH_2P_2O_7$. Ions replacing a larger ion, however, eg magnesium in $CaH_2P_2O_7$ have lower than ideal BV values. These values support the strong dependence of the structure on size and indicate the instability of too large or small a replacement cation at a given site.

3.3 Summary

The synthesis and structure determination of magnesium acid pyrophosphate $MgH_2P_2O_7$, was achieved. The doping of calcium and magnesium acid pyrophosphates was attempted, but there was no conclusive evidence that doping was occurring. This may be due to the stability of these structures being strongly linked to the size of the cation, so much so that even small levels of doping are prohibited.

3.4 References

1 M. Alvarez-Vega, O. Garcia-Moreno, F. Garcia-Alvardo, J. Garcia-Jaca, J. M. Gallardo-Amores, M. L. Sanjuan and U. Amador, *Chem. Mater.* 2001, **13**, 1570−1576

2 G. Alberti, M. Casciola, U. Costantino, and R. Vivani, *Adv. Mater.* 1996, **8**, 291−303

3 J. M. M. Millet, *Catal. Rev.* 1998, **40**, 1−38

4 P. Bonnet, J. M. M. Millet, C. Leclercq and J. C. Vedrine, *J. Catal*. 1996, **158**, 128−141

5 J. Trommer, M. Schneider, H. Worzala and A. N. Fitch, Ed: R. Delhez and E. J. Mittemeijer, *European Powder Diffraction, Pts 1 and 2*, 2000, **321-3**, 374-379

6 CRYSFIRE Suite: R. Shirley, The CRYSFIRE System for Automatic Powder Indexing.

7 T. Yang, J. Ju, G. Li, S. Yang, J. Sun, F Liao, J. Lin, J. Sasaki and N. Toyota, *Inorg. Chem.* 2007, **46**, 2342-2344

8 A. J. Wright and J. P. Attfield, *Inorg. Chem.* 1998, **37**, 3858-3861

9 J. Trommer, M. Schneider, H. Worzala and A. N. Fitch, *Mater. Sci. Forum*, 2000, **321**, 374-379

10 H.-S. Ryu, K. S. Hong, J.-K. Lee, D. J. Kim, J. H. Lee, B.-S. Chang, D.-H. Lee, C.-K. Lee and S.-S Chung, *Biomaterials*, 2004, **25**, 393–401

11 E. J. Kim, S.-W. Choi and Seong-Hyeon Hong, *J. Am. Ceram. Soc.* 2007, **90**, 2795–2798

12 J.W. Reida, A. Pietaka, M. Sayera, D. Dunfielda and T.J.N. Smith, *Biomaterials* 2005, **26**, 2887-2897

13 Y. W. Chen, G. Q. Shi, Y. L. Ding, X. X. Yu, X. H. Zhang, C. S. Zhao and C. X. Wan, *J. Mater Sci. Mater. Med.* 2008, **19**, 2655–2662

14 L.E. Jackson and A. J. Wright, *Bioceramics 17*, 2005, **284-286**, 71-74

15 J. Laugier and B. Bouchu http://www.ccp14.ac.uk/tutorial/lmgp/index.html#chekcell retrieved December 2009

Chapter 4: A Biologically Inspired Organic/Inorganic Composite

4.1 Introduction

Polyhydroxybutyrate (PHB), shown in Figure 20 a, is found in all living cells. Indeed, up to 70% of the dry weight of cells can be composed PHB granules. It has been suggested that it is used as an energy store by prokaryotic cells when they are in nutrient-poor conditions[1].

Complexes of calcium polyphosphate (Ca PolyP) and PHB have been found in cell walls[2,3,4]. The structure of these complexes and the interaction between the inorganic and organic components are uncertain. The aim of this part of the project was to investigate the effect of PHB or its monomer, hydroxybutyrate (HB), shown in Figure 20 b, on the formation of γ-CaPolyP. In particular we were interested in looking for stability changes in γ-CaPolyP phases and for new phases, which include the organic functionality, which may provide information on the structure of possible complexes.

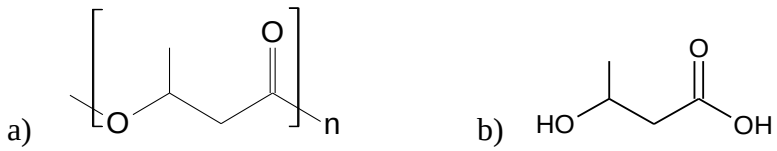

Figure 20: Structure of a) polyhydroxybutrate (PHB, $(C_4H_6O_2)_n$) and b) its monomer, hydroxybutrate (HB, $C_4H_6O_8$).

To explore the potential for forming composites of Ca PolyP and PHB or HB a range of

syntheses were employed. Calcium polyphosphates are commonly formed by two methods; firstly by decomposition of an appropriate precursor and secondly by phosphoric acid fluxes. Both were used in the work described in this chapter, but the synthesis was modified by the presence of PHB and/or HB.

4.2 Experimental

The experiments reported here used the sodium salt of HB, Na HB, which has the structure shown in Figure 21.

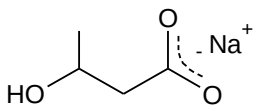

Figure 21: The structure of Na HB.

Precursor method: equal amounts (1 g) of monocalcium phosphate monohydrate (MCPM, $Ca(H_2PO_4)_2.H_2O$) and PHB or Na HB were ground together. They were then heated in a porcelain crucible at 150, 200 and 250°C for between 1 and 12 h.

Acid melt: an excess of phosphoric acid was mixed with 0.96 g calcium hydroxide and 0.96 g PHB or Na HB in a porcelain crucible. The calcium:phosphorus ratio used was 1:4. The samples were then heated to between 250 and 400°C for 12 h. When the samples had cooled they were washed with distilled water to remove any excess phosphoric acid and dried at 40°C for 3 h.

When Na HB was used, experiments were also undertaken using NaOH to determine if the presence of the sodium ions rather than the HB was responsible for any change in the final product.

4.3 Results and Discussion

4.3.1 Decomposition of Precursor MCPM

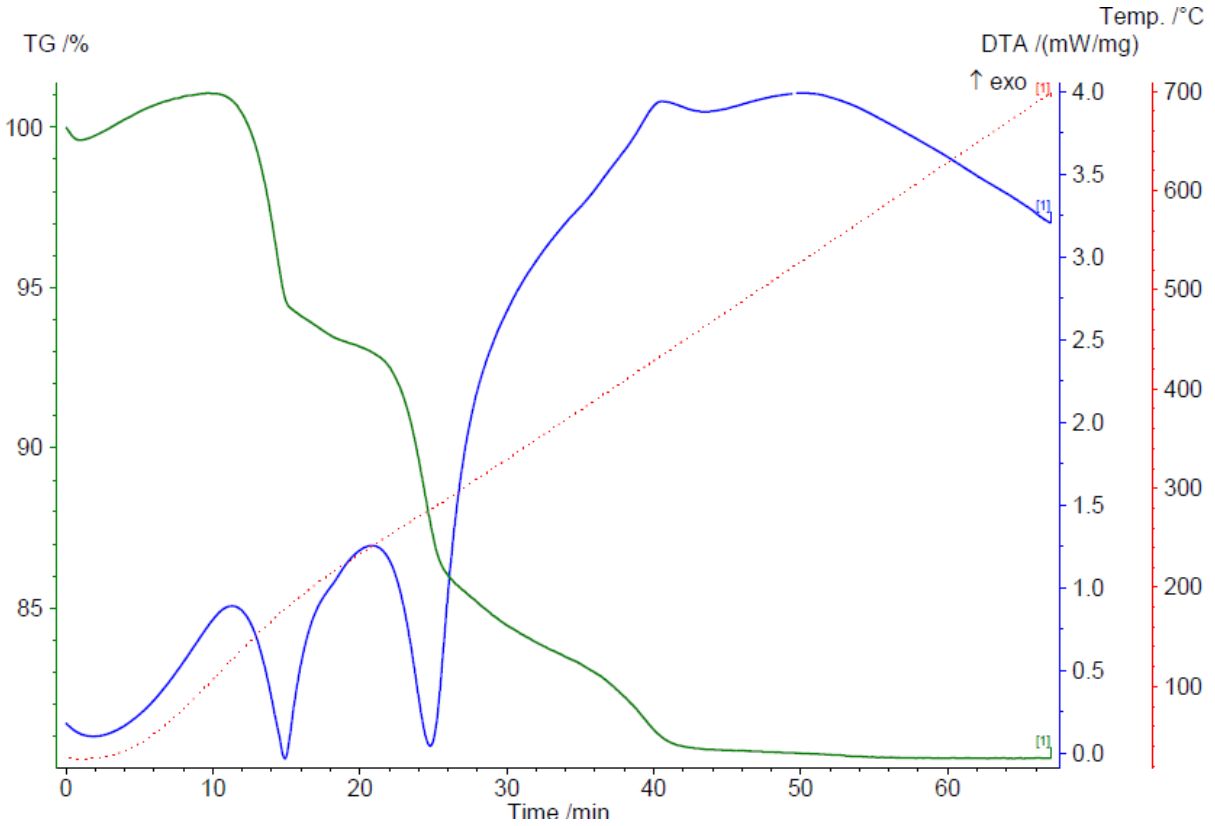

Figure 22: TG/DTA trace for MCPM heated to 700°C. The weight change is shown in green and the heat flow in blue.

The decomposition of MCPM to provide calcium polyphosphates was investigated previously

by Webb[5]. The initial experiments sought to confirm the decomposition pathway reported by Webb, then to investigate whether the approach could be modified to produce a composite product.

Using TG/DTA data, shown in Figure 22, it was demonstrated that, between 125 and 180°C, MCPM dehydrated to form monocalcium phosphate (MCP, $Ca(H_2PO_4)_2$). The 7% weight decrease was consistent with the loss of one formula unit of water. The next endothermic event was the formation of γ-CaPolyP (γ-$Ca(PO_3)_2$) between 255 and 290°C, which coincided with another weight loss. Between 390 and 420°C there was an exothermic event which was identified as the formation of β-CaPolyP. The weight loss during the formation of CaPolyP was consistent with the loss of two units of water corresponding to the formation of $Ca(PO_3)_2$ from $Ca(H_2PO_4)_2$.

$$\text{MCPM} \xrightarrow[-H_2O]{125\,^\circ\text{C}} \text{MCP} \xrightarrow[-2H_2O]{255\,^\circ\text{C}} \gamma\text{-CaPolyP} \xrightarrow{390\,^\circ\text{C}} \beta\text{-CaPolyP}$$

Scheme 1 : Reaction scheme for formation of γ-CaPolyP and β-CaPolyP from MCPM.

Variable temperature XRPD was used to investigate the transformations up to a temperature of 300°C. This is below the decomposition temperature of PHB and so a viable regime for a composite reaction. An XRPD pattern was measured every 25°C. This data, reported in, shows the formation of MCP from MCPM between 100 and 125°C, which is consistent with the formation temperature, measured using TGA. The XRPD pattern for dehydrated MCPM matched an indexed pattern[6] of MCP (MCP 1). At 275°C the MCP forms a largely amorphous

phase as shown in result 7 in Figure 23. At higher temperatures calcium polyphosphate is formed.

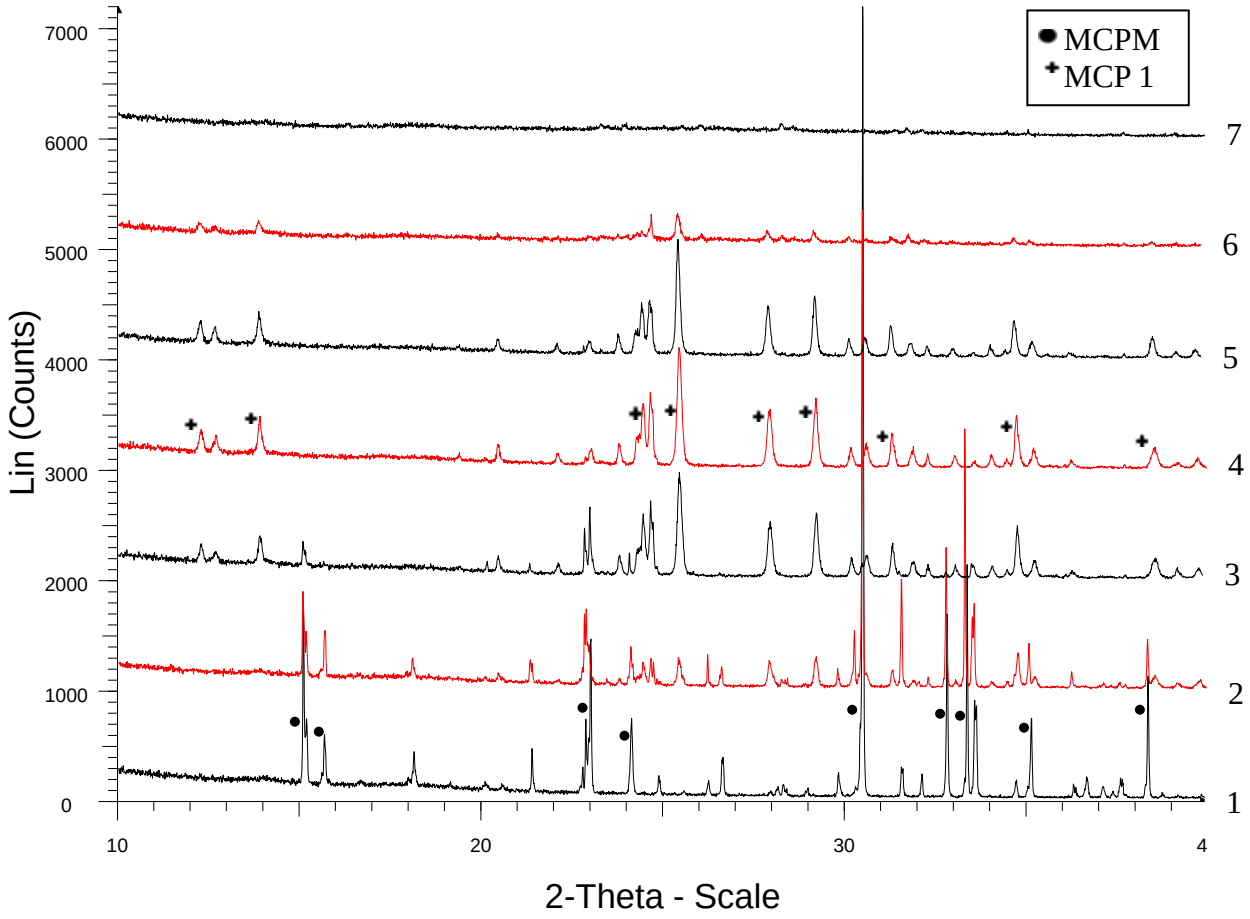

Figure 23: Variable temperature XRPD pattern of MCPM. Temperatures from bottom to top, 1) 25°C, 2) 125°C, 3) 150°C, 4) 175°C, 5) 250°C, 6) 275°C and 7) 300°C. The main MCPM peaks are identified by circles and peaks corresponding to MCP 1 by crosses to the left of the peaks.

4.3.2 Attempts at Forming a Polyphosphate/PHB Composite Via the Precursor Synthesis

The next aim of this work was to produce a composite between inorganic calcium phosphates

and an organic polymer, PHB. Any composites, which were formed could be used to explore the chemical interactions between the inorganic and organic components. Moreover, if they had the necessary physical properties, their potential as biomaterials could be considered.

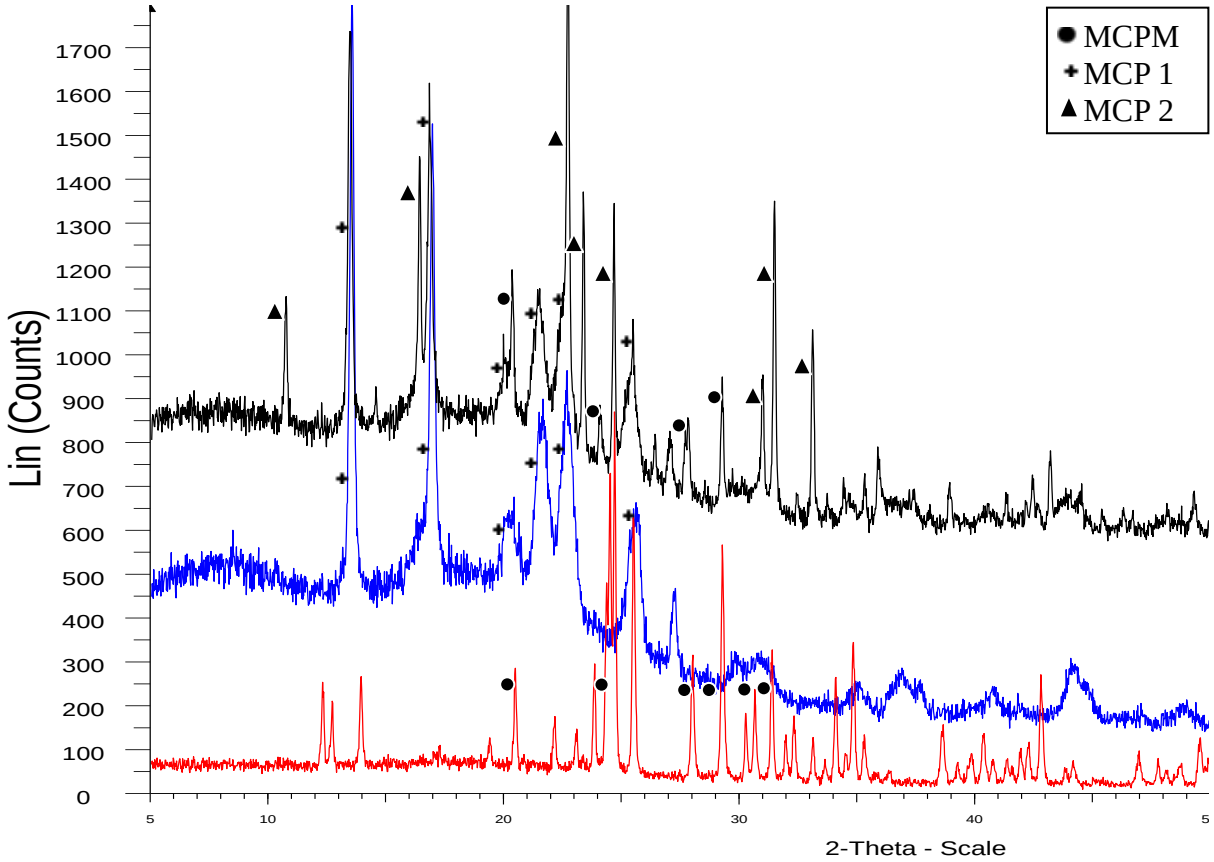

Figure 24: XRPD data of samples heated at 150°C for 12 h. Bottom: PHB only; middle: MCPM only and top: MCPM and PHB. The main PHB peaks are identified by circles, MCP 1 by crosses and to MCP 2 by triangles to the left of the peaks.

To investigate whether a composite could be formed, we collected XRPD data for PHB, for MCPM, and for a mixture of the two compounds. The samples were heated at 150°C for 12 h and the results are shown in Figure 24. In agreement with the variable temperature XRPD when MCPM was dehydrated at 150°C it formed MCP 1. When PHB was added to the

reaction, the XRPD data shows that another polymorph of MCP (MCP 2) was formed as well as MCP 1. This form of MCP has been reported before[51], but its structure is unknown. The reason a different polymorph was formed in the presence of PHB is unclear, the organic component could be templating the formation of MCP 2, or its presence could change the physical conditions in the reaction vessel. As shown in Figure 24, the PHB does not completely decompose during the reaction. When PHB only was heated at 150°C there was a slight increase in crystallinity.

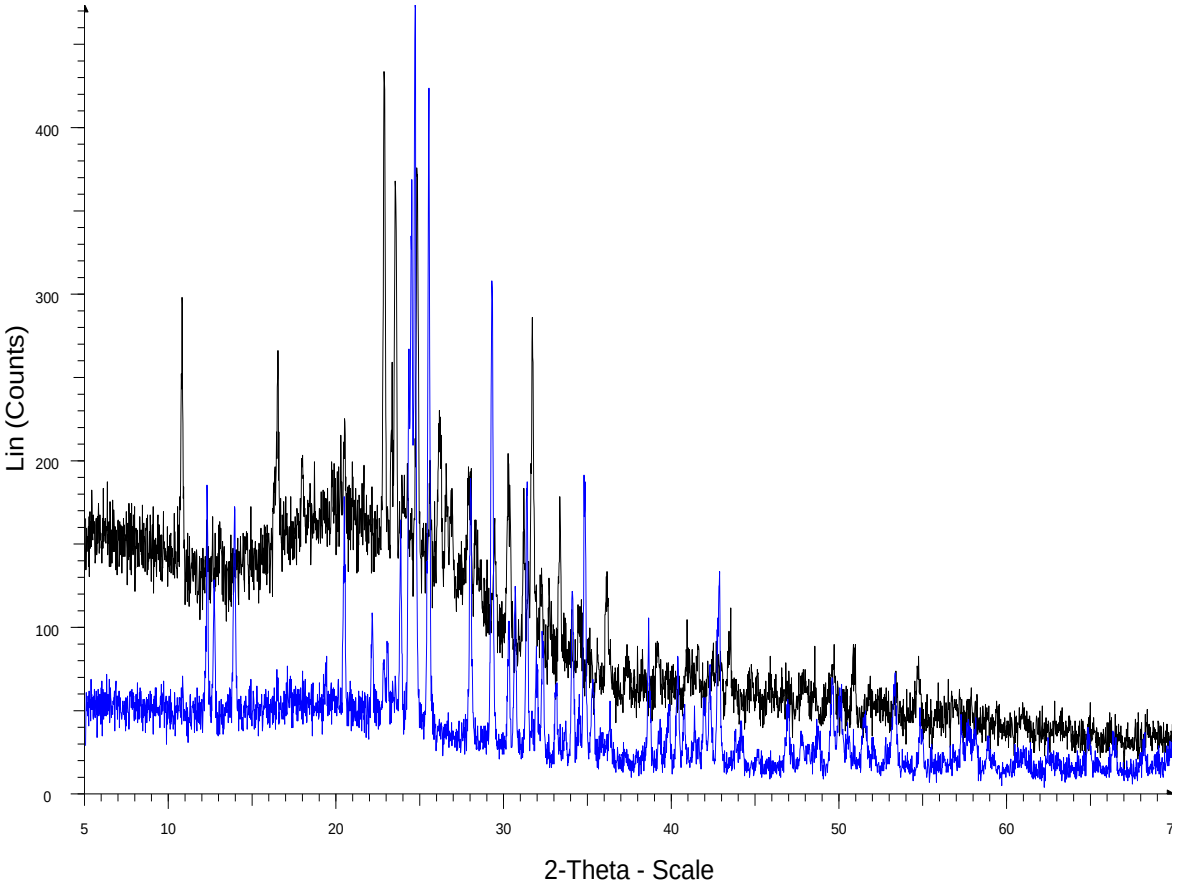

Figure 25: XRPD data for samples heated at 200°C for 12 h. Bottom: MCPM only and top: MCPM and PHB. All the peaks in the MCPM only pattern are from MCP 1 and all the peaks in the MCPM and PHB pattern are from MCP 2.

Figure 25 compares the XRPD data after heating for 12h at the higher temperature, 200°C. The crystalline MCP products were the same as at 150°C, MCP 1 for the MCPM only sample and MCP 2 for the sample containing PHB. There was, however, more amorphous material present, especially in the sample containing PHB. At this temperature there were no PHB peaks present in the XRPD patterns showing that all the PHB had decomposed.

When samples of MCPM, both with and without PHB, were held at 250°C the products were mostly amorphous. This is consistent with previous work on the decomposition of MCPM[51].

The thermal decomposition of PHB has been previously studied by Grassie et al[7]. Their TGA data showed that PHB decomposed between 250 and 300°C. The lower decomposition temperature reported here is probably due to the increased heating time. Grassie used a constant heating rate of 10°C/min. In our experiments the samples were heated to their final temperature at a similar rate, but they were then held at that temperature for 12h.

PHB decomposed at around 200°C, lower than the temperature at which γ-Ca PolyP is formed. Therefore it was not possible to from a composite via this route. Another attempt was made to study the reaction using the PHB monomer HB.

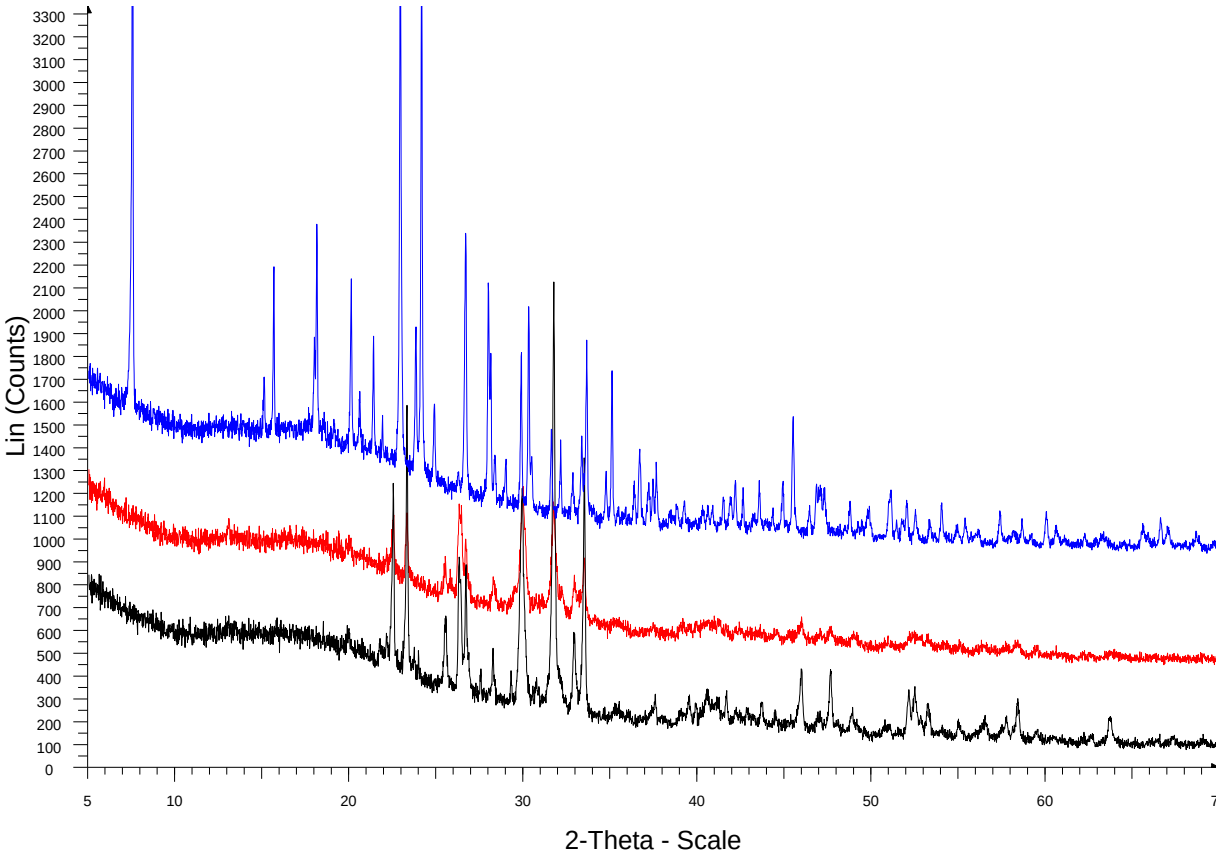

Figure 26: XRPD data of samples heated at 150°C for 12 h. Bottom: MCPM and Na HB, middle: NaOH and MCPM and top: MCPM only

Samples of MCPM mixed with Na HB were heated at 150, 200 and 250°C for 12h. MCPM and NaOH samples were also reacted to determine whether the sodium ions or the organic components were affecting the product. Typical results, for 150°C, are shown in Figure 26. The main crystalline products were the same for all the samples containing added reagents, but were not identified. The amount of amorphous products present increased, as expected, with increasing temperature, with more amorphous products in the samples containing NaOH for all temperatures. In the Na HB samples the Na HB completely decomposed when heated at 200°C or above. The presence of the same unidentified products indicates that it is likely

that the sodium ions are determining the product that is formed rather than the organic monomer. We may therefore infer that we have been unsuccessful in producing a composite phase via this route.

4.3.3 Attempts at Forming a Polyphosphate/PHB Composite Via the Acid Melt Synthesis

An acid melt synthesis was also investigated as a route to the formation of a PHB/Ca PolyP composite. At 150°C, a mixture of phosphoric acid and calcium hydroxide is known to form calcium acid pyrophosphate ($CaH_2P_2O_7$). Reactions performed with Na HB present displayed no change in the observed product and there was no evidence of an organic-containing product being formed. This was probably due to the HB remaining in the unreacted phosphoric acid.

When PHB was used instead of the monomer HB, the product obtained was amorphous. At 150°C PHB would not be expected to decompose. It is likely that the presence of the large PHB molecules affected the precipitation of calcium phosphates, preventing the formation of any crystalline product. Alternatively the acidic conditions may have caused the breakdown of the PHB into smaller polymers units at lower temperatures than expected. These smaller polymers would be unlikely to be crystalline and would again prevent the crystallisation of calcium phosphate.

4.4 Conclusions

The original aim of this part of the project was the formation of an inorganic/organic composite via chemical methods. Successful composites between γ-CaPolyP and PHB were not achieved using the methods reported here, the solid state precursor method or the acid melt synthesis, due to the low decomposition temperature of PHB.

Further attempts were made to study the interactions between the organic and inorganic components using the PHB monomer HB. Any effects due to the organic component were difficult to determine as the sodium salt was used for experiments. It also was found to have too low a decomposition temperature to investigate interactions with γ-CaPolyP.

4.5 References

1 Y. Doi. *Microbial Polyesters*; VCH: New York, 1990

2 R. N. Reusch, R. Huang, and L. L. Bramblet, *Biophys. J.* 1995, **69**, 754-766

3 R. N. Reusch and H. L. Sadoff, *Proc. Nat. Acad. Sci. USA*, 1988, **85**, 4176-4180

4 D. Seebach, H. M. Burger, H.-M. Miller, U. D. Lengweiler and A. K. Beck, *Helv. Chim. Acta*, 1994, **77**, 1099-1123

5 L. E. Webb, PhD Thesis, University of Birmingham, 2007

6 J. P. Smith, J. R. Lehr and W. E. Brown, *Am. Mineral*, 1955, **40**, 893-899

7 N. Grassie, E. J. Murray and P. A. Holmes, *Polym. Degrad. Stab.* 1984, **6**, 47-61

Chapter 5: Synthesis of Aligned Calcium Polyphosphate Crystals

In chapter 5 the attempt to syntheses aligned calcium polyphosphate crystals on magnetic and charged piezoelectric surfaces is reported. The synthesis of aligned crystals would allow testing of any piezoelectric and pyroelectric properties γ-calcium polyphosphate.

5.1 Introduction

γ-calcium polyphosphate (γ-Ca PolyP) has an unusual crystal structure with layers of helical chains stacked in alternating perpendicular directions. It has a non-centrosymmetric and polar space group (monoclinic, Cc) which suggests it may possess piezoelectric or pyroelectric properties. A piezoelectric material is a material which has the ability to develop an electric field when a mechanical stress is applied. A pyroelectric material will develop an electric field when it is heated or cooled. Bone has been found to have a small piezoelectric effect which may be important in growth of new bone[1]. Clearly, if this is important, it would be advantageous for a replacement material to be able to promote the growth of new bone by developing a small electric charge in the same way as natural bone.

Surprisingly little research has been directed to the dielectric properties of bones or of possible replacement materials. It has been shown that bone growth is accelerated on the negatively charged surface of polarized hydroxyapatite (HA)[2]. The mechanism for the acceleration of growth is not known, but it has been speculated that it is due to the adsorption of calcium (II) ions, which act as nucleation sites for calcium phosphate. There have been studies of composites of HA and ferroelectric materials such as barium titanate ($BaTiO_3$)[3,4]. It

was however found that, for the composite to have measurable piezoelectric properties, the percentage of ferroelectric material it contains needs to be very high, 80% in the case of barium titanate[51]. The reduction in the piezoelectric effect of the barium titanate in complexes may be due to the presence of HA causing matrix clamping or barium/calcium ion substitution. Most ferroelectric materials contain ions, which are not cytocompatible and so their use in composites is limited. The synthesis of cytocompatible or biocompatible piezoelectric materials would clearly be advantageous.

γ-calcium polyphosphate is a rare (if not unique) example of a calcium phosphate with a polar space group. To test for a piezoelectric effect in this phase either requires a sufficiently large single crystal to be grown or a polycrystalline sample containing fused orientated crystallites. If a sample of randomly orientated crystallites is used, the field that develops across each individual crystallite will be in a different direction and will lead to cancellation. If a sample with orientated crystallites is used the field developed across each one will be in the same direction and will reinforce to create an overall field.

The formation of crystals of a piezoelectric material may be affected by the presence of an electric or magnetic field. There has been some work into the precipitation of crystals from solution at room temperature in an electric field[5] or a magnetic field[6]. Both studies showed that the fields have an effect on the morphology or orientation of the crystals formed. Crystals of calcium phosphates have been grown from a saturated solution of HA on charged and uncharged piezoelectric plates[7]. The charged plates had a weak electric field around them. More crystals formed on negatively charged plates than positively charged or uncharged plates. The crystals on the negative plates were aligned, whereas on other plates they were

randomly oriented.

γ-Ca PolyP can be formed via the decomposition of monocalcium phosphate monohydrate (MCPM). In its formation, the structure of MCPM will completely rearrange to form the new γ-Ca PolyP structure. This should allow any crystals that form to orientate with the external field surrounding the sample if any alignment effect is sufficiently strong. The methodology chosen was to place pellets of MCPM onto charged and uncharged piezoelectric materials, onto strong permanent magnets and, as controls, onto alumina surfaces. Samples were heated to convert the MCPM to γ-calcium polyphosphate and XRPD was used to monitor for any orientation effects. Pellets were used as the samples had to be robust enough to withstand any piezoelectric testing.

5.2 Experimental

5.2.1 Formation of Precursor Pellets

Pellets of 0.4 g of MCPM were used. They were heated to allow the formation of γ-Ca PolyP. When MCPM is heated to form γ-Ca PolyP, three formula units of water are lost. This water loss could cause the pellets to deform or disintegrate. It was found that a good method for forming the pellets was to use 2 tons of pressure and to make them relatively thin, about 0.8 mm. After heating the pellets were strong enough to withstand the piezoelectric testing.

$CaH_2P_2O_7$ was also used as a precursor material as the loss of only one unit of water would cause less disruption to the pellet. When the first pellets were made the sample used was

hydrated and contained too much water to form a stable pellet. Alternative samples which had been stored in a desiccator were successfully made into pellets using the same method as for MCPM.

5.2.2 Choice of Dielectric and Magnetic Materials

Both magnets and charged piezoelectric materials have a Curie temperature above which the magnetisation or the polarization is lost. The temperature that MCPM needs to be heated to for γ-Ca PolyP to form is at the limits of the stability of the piezoelectric materials and the magnets used. The permanent magnets used were AlNiCo (an alloy of aluminium, nickel and cobalt) and SmCo (an alloy of samarium and cobalt) with maximum working temperatures of 550 and 120°C respectively[8]. The piezoelectric materials used were PZT (lead zirconate titanate, $Pb(Zr_xTi_{1-x})O_3$ $0 < x < 1$) and NKN (sodium potassium niobate $(Na_{0.5}K_{0.5})NbO_3$)) with Curie temperatures of approximately 330°C (the exact value depends on the ratio of zirconium to titanium)[9] and 415°C[10] respectively.

5.3 Results

5.3.1 Establishing Optimum Reaction Conditions

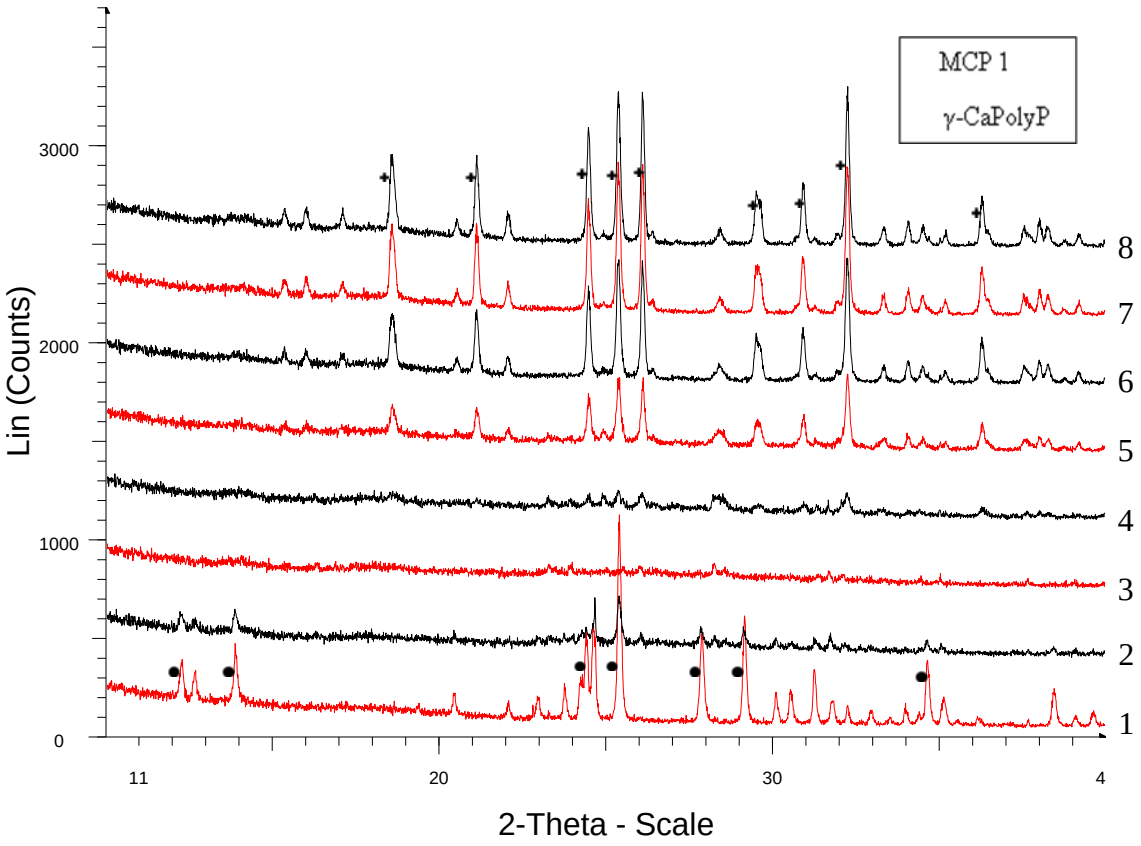

Figure 27: Variable temperature XRPD of MCPM. Temperatures from bottom to top, 1) 250°C, 2) 275°C, 3) 300°C, 4) 325°C, 5) 325°C after heating for 40 min, 6) 325°C after 80 min, 7) 325°C after 120 min 8) 325°C after 160 min. The main MCP 1 peaks are marked with a circle and the main γ-Ca PolyP peaks with crosses to the left of the peaks.

A variable temperature XRPD experiment was undertaken to find the optimum temperature and heating rate for the conversion of MCPM to γ-Ca PolyP. Scans were taken every 25°C between 250 and 325°C. The temperature was then kept at 325°C and a scan taken every 40 minutes. The results, collected in Figure 27, showed a transition from monocalcium

phosphate (MCP 1) to γ-Ca PolyP via an amorphous phase. γ-Ca PolyP first started to form when the temperature was at 325°C, and the amount of crystalline material increased to a maximum after 160 min of heating.

A number of experiments were then undertaken to determine whether these heating rates would be suitable for use with pellets. It was found that the pellets formed γ-Ca PolyP more slowly than the powder sample used in the variable temperature XRPD so the length of time at 325°C was increased. It was initially found that the optimum conditions were to heat at a rate of 0.6°C/min to 325°C and then heat at 325°C for 6 h. There was no reduction in the magnetisation of the magnets, and only a small reduction in the polarization of the piezoelectric materials, for this heating protocol so experiments with a slower heating rate (0.3°C/min) were performed to try to increase the size of crystals formed and to reduce the amount of amorphous material in the pellets.

To establish the success of the experiments, samples were removed from the surface of the ferroelectric and magnetic materials and then examined by reflection XRPD. We hoped that any preferred orientation of crystals within the material would be evidenced by changes in the intensity of some reflections when compared to the sample heated on the control (alumina). The particular reflections that change intensity will signify the direction which the crystals are preferentially orientated along.

All the ferroelectric, magnetic and alumina substrates were microcrystalline. The irregular microcrystalline surfaces should not produce any noticeable structural templating effect. Changes in intensity should therefore be due to the effect of the electric or magnetic fields on

the orientation of the calcium polyphosphate product.

5.3.2 MCPM Pellets Heated on Magnets

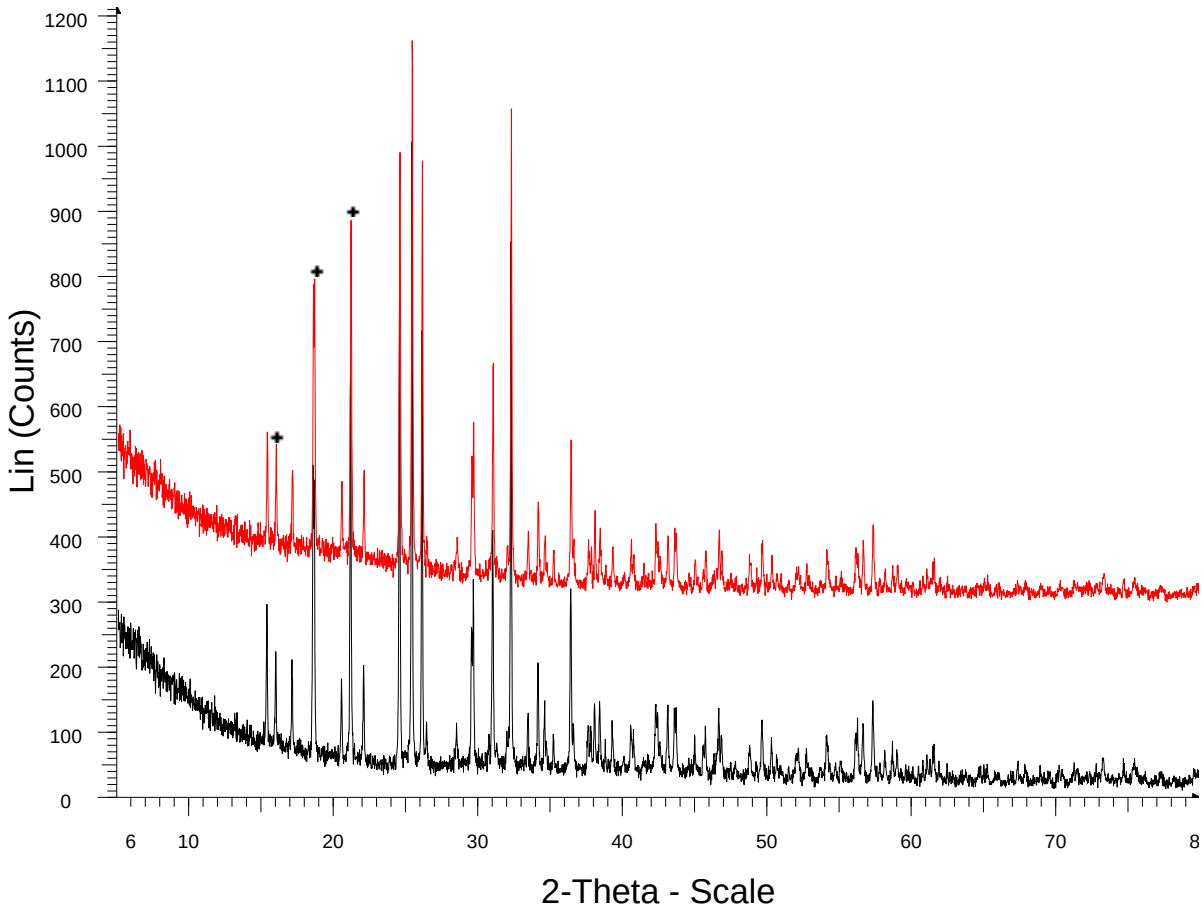

Figure 28: XRPD data of MCPM heated at a rate of 0.6°C/min bottom: on alumina and top: on an AlNiCo magnet. The peaks with the most significant changes in intensities are marked with a cross above the peaks.

We first describe results for pellets heated on magnets. Figure 28 compares the XRPD spectrum for pellets heated on a magnetic substrate and on an alumina control. The comparison between the XRPD patterns shows there are some differences in intensity that may indicate some crystal alignment. The main peaks that show greater intensity for the

magnet than for the alumina control are those at $2\theta \sim 16°$, 19° and 21° (marked with a cross) which correspond to the (111), (020) and (−112) planes respectively. However, the analysis did not show any correlation in direction which could cause the increased intensity of these particular peaks. Therefore we were unable to show the magnetic surface had any effect on the alignment of the crystals.

5.3.3 MCPM Pellets Heated on Piezoelectric Materials

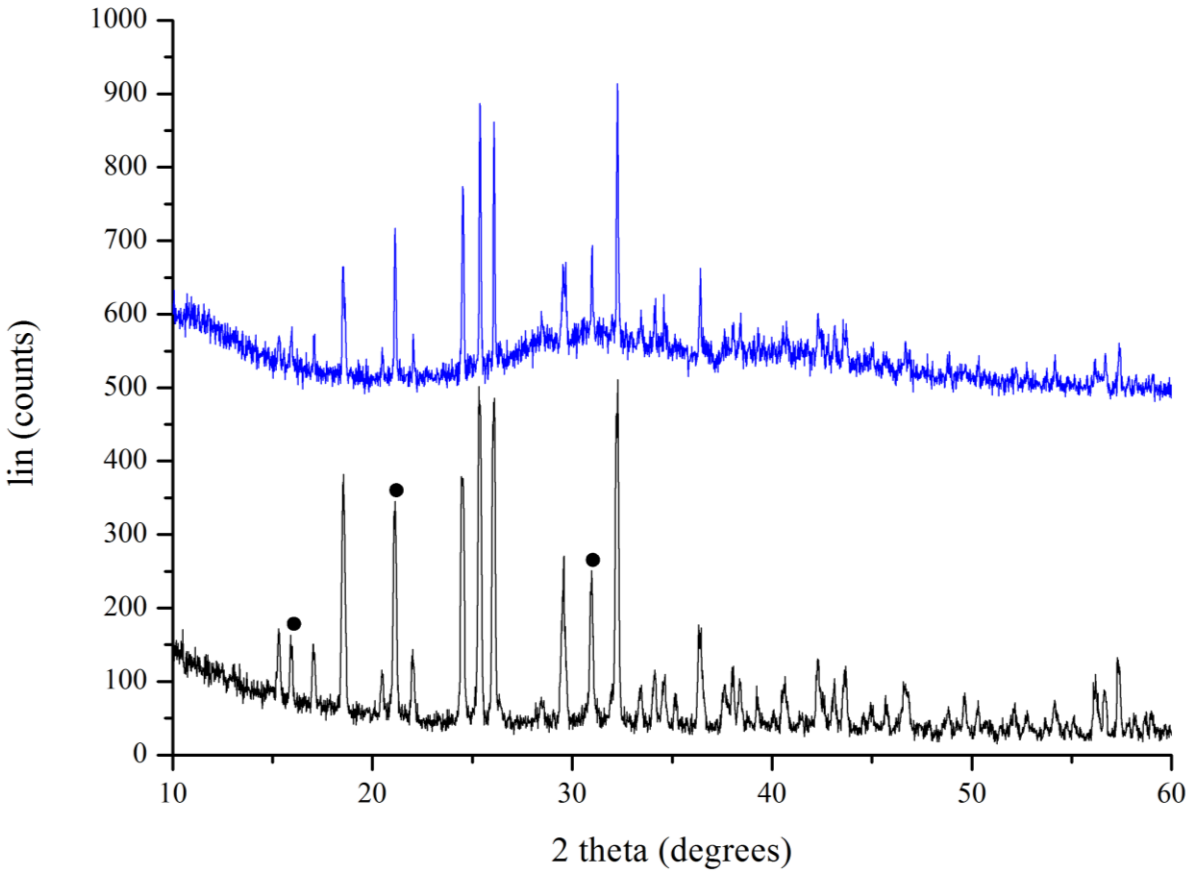

Figure 29: XRPD data of MCPM heated at a rate of 0.6°C/min on charged, gold coated PZT (top) and on alumina (bottom). The peaks with the most significant changes in intensity are marked with a circle above the peaks.

The pellets which were heated on piezoelectric materials have much higher levels of amorphous material than the samples heated on magnets. Indeed pellets on silver coated and uncoated NKN had effectively no crystalline material. The effect may be due to the electric field around the material or the polycrystalline ceramic may template the formation of the calcium phosphate. The former is more likely, as the samples were in pellet form, so there was minimal contact with the surface. Moreover the effect was the same on coated and uncoated samples and the control sample on alumina (a similar ceramic surface) had much lower levels of amorphous material.

On a PZT substrate, however, there was some crystalline product. The XRPD pattern of MCPM pellets heated on both alumina and gold coated PZT show some peaks which are more intense than the control. This is shown for the gold substrate and control data on alumina for comparison is shown in Figure 29. The most significantly increased peaks are those at $2\theta = 16°$ (111), 21° (–112) and 31° (–222). However again these do not correspond to a discernable preferred direction.

5.3.4 $CaH_2P_2O_7$ Pellets Heated on Magnets

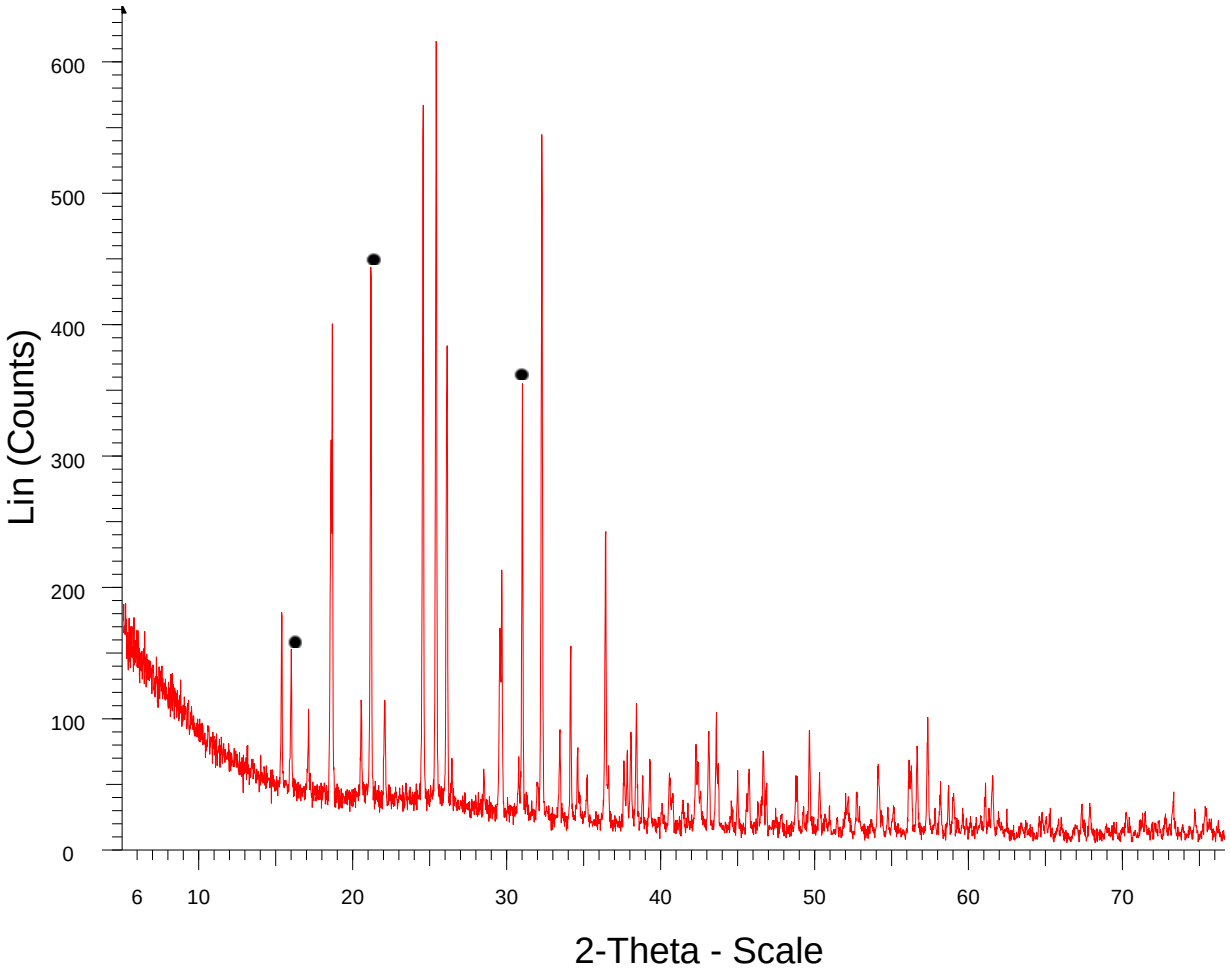

Figure 30: XRPD data of $CaH_2P_2O_7$ heated at a rate of 0.6°C/min on an AlNiCo magnet. The peaks with the most significant changes in intensity are marked with a circle above the peaks.

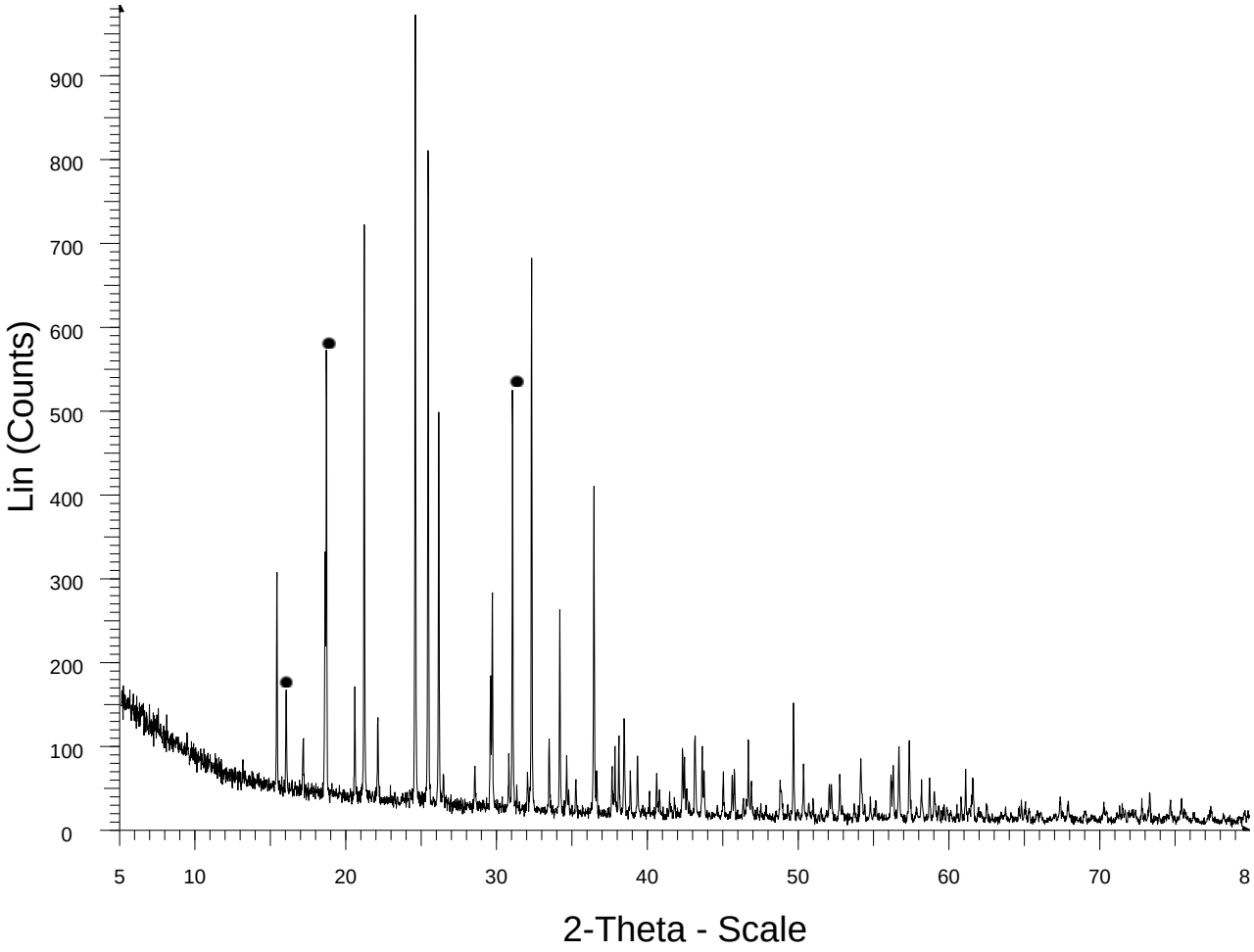

Figure 31: XRPD data of $CaH_2P_2O_7$ heated at a rate of 0.6°C/min on alumina. The peaks with the most significant changes in intensity are marked with a circle above the peaks.

Pellets made from $CaH_2P_2O_7$ were also heated, using the same heat rate, on AlNiCo. This compound loses less water when forming γ-Ca PolyP and so there will be less disruption to structural properties of the pellets. The XRPD data shown in Figures 30 and 31 Figure show that the resulting γ-Ca PolyP did contain a lower level of amorphous material than that produced from pellets made of MCPM. The peaks which have higher intensities in the sample on the magnetic substrate, when compared to the control, are at 2θ = 16° (–111), 19° (–122) and 31° (–222). The peak at 24.5° (–202) is significantly weaker than the peak in the alumina

sample.

There are peaks which have higher intensity in one or more of the experiments results, for example the peak at 16° (–111) is more intense on both the magnetic and piezoelectric substrates. However the lack of a clear correlation between the enhanced peaks indicates that, even though the fields appear to be having some effect on the formation of the crystals, this has, as yet, not been identified as an alignment effect.

5.4 Conclusions

The aim of this chapter was to align γ-Ca PolyP crystals in order to measure their piezoelectric properties. The ideal heating rate for the synthesis of γ-Ca PolyP was determined, and magnetic and piezoelectric substrates which would remain polarized at the necessary temperatures were chosen. Pellets of MCPM and $CaH_2P_2O_7$ were heated on charged and uncharged piezoelectric materials and strong permanent magnets. After heating the pellets were analysed using reflection XRPD. There were some changes in the peak intensities of pellets heated on the active substrates compared to those on alumina controls, but it has not yet been possible to quantify or explain this effect.

5.5 References

1F. Jianqing, Y. Huipin and Z. Xingdong, *Biomaterials*. 1997, **18**, 1531-1534

2 R . Kato, S. Nakamura, K. Katayama, and K. Yamashita, *J. Biomed. Mater. Res.* 2005, **74A**, 652,

3 F. Jianqing, Y. Huipin and Z. Xingdong, *Biomaterials* 1997, **18,** 1531-1534

4 J. P. Gittings, C. R. Bowen, I. G. Turner, F. Baxter and J. Chaudhuri, *J. Eur. Ceram. Soc.* 2007, **27**, 4187–4190

5 G. J. Evans, *Mater. Lett.* 1984, **2**, 420-423

6 K. Higashitani, A. Kage, S. Katamura, K. Imai and S. Hatade, *J. Colloid Interface Sci.* 1993, **156**, 90-95

7 X. Sun, C. Ma, Y. Wang and H. Li, *J. Cryst. Growth.* 2002, **234**, 404–410

8 http://www.magdev.co.uk/index.aspx Retrieved 19th Decemember 2009

9 E. Sawaguchi, *J. Phys. Soc. Jpn.* 1953, **8**, 615-629

10 Y. Saito, H. Takao, T. Tani, T. Nonoyama, K. Takatori, T. Homma, T. Nagaya and M. Nakamura, *Nature*. 2004, **432**, 84-87

Chapter 6: Summary and Further Work

6.1 Summary

This thesis presents new work on various forms of condensed phosphate. The structure of $MgH_2P_2O_7$, obtained from its XRD pattern by a Rietveld refinement based on $NiH_2P_2O_7$, is reported for the first time. The structure has zigzags of magnesium – oxygen octahedra linked by pyrophosphate groups. The bond lengths and angles are comparable to other magnesium phosphates.

The doping of $CaH_2P_2O_7$ (with Mg and Sr ions) and $MgH_2P_2O_7$ (with Ca ions) was then investigated. There was no conclusive evidence that doping was occurring. Bond valence calculations showed that the sites were very size-dependent so that a larger or smaller atom on a site is likely to be unstable. If doping did occur it had a very low saturation level.

The second section of the thesis focused on γ-calcium polyphosphate (CaPolyP) and its use as a biomaterial. In light of the interaction between Ca PolyP and PHB in the cell membrane, an attempt was made to produce a composite. The low decomposition temperature of PHB meant that this was not possible. PHB was, however, found to affect the dehydration of MCPM to form MCP. The possibility of using a sodium salt of a monomer of PHB, HB, to form a composite was also studied. However, any effects were attributed to the presence of sodium in the sample rather than the presence of the HB.

The effect of magnetic fields and electric fields on the growth of γ-CaPoly crystals was

studied in an attempt to create pellets of aligned crystals. The formation of aligned crystals would have allowed the piezoelectric properties of the samples to be measured. PXRD was used to analyse pellets, but there was little evidence that the fields had any effect on formation of the crystals.

6.2 Further work

6.2.1 Doped $CaH_2P_2O_7$

Further work, such as carefully calibrated XRF, needs to be undertaken to definitely determine if doping of $CaH_2P_2O_7$ is occurring. Doping with other ions of a similar size could also be attempted. However when choosing the dopant ions the ultimate aim of producing biomaterials needs to be considered: the ions must be cytocompatible if they are to be released into the body. For example, if 1+ or 3+ ions are used, counterbalancing ions must also be added to maintain the charge balance.

Doping γ-CaPolyP using an acid melt synthesis did not work. Using a solid state method to form doped samples is often more successful than an acid melt, as less favourable ions cannot be left in the excess phosphoric acid. Although the initial attempts were unsuccessful, further investigations into the acid melt method were planned. However, it was not possible to perform the experiments for this thesis due a fault with the equipment.

6.2.2 γ-Calcium polyphosphate and Polyhydroxybutrate

Alternative methods to form composites are physical routes such as ball milling. This would allow the formation of a γ-CaPolyP and PHB composite despite the low decomposition temperature of PHB. However, physical routes would not produce composites with chemical interaction, which was the original aim of the project. More work could also be done using hydroxybutyrate or its calcium salt.

The use of similar polymers could also be explored: PHBV, a copolymer of PHB and polyhydroxyvalerate (PHV) have slightly higher melting and boiling points than PHB. Polymers which contain ester groups (polyesters) could also be investigated.

It would be interesting to study the interactions between the calcium phosphate and PHB by isolating the biological complexes from cell walls. This might help to understand how to synthesise a suitable composite.

6.2.3 Synthesising Aligned Crystals

The next step in trying to produce aligned γ-CaPoly crystals would be to perform the synthesis in higher electric and magnetic fields to increase any effect of the fields. This would require building equipment which could safely produce the necessary fields at in ovens at high temperatures. The main problems are using high electric fields in humid conditions and finding suitable configurations for setting up charged plates or electromagnets in an oven and connecting them to a power source. Wires and any insulation would have to withstand the

required temperatures.

Work exploring using acid melt synthesis to produce aligned crystals could also be performed. In the absence of a field, γ-CaPolyP forms an agglomeration of small crystals. A field might cause the aligned formation and precipitation of the crystals. The method would, however, then have to be modified, as normally the crystals would be washed to remove any unreacted acid which would destroy the alignment. Moreover, the crystal agglomerations may not be strong enough to withstand the piezoelectric testing.

Appendix A: Structural data for $MgH_2P_2O_7$

Table 6: Crystallographic data for $MgH_2P_2O_7$

Empirical formula	$MgH_2P_2O_7$
Formula weight	216.04
Crystal system	Monoclinic
Space group	$P2_1/c$
a	9.0209(1) Å
b	12.7095(1) Å
c	9.6083(1) Å
β	106.15(5)°

Table 7: Atomic coordinates of the atoms in a unit cell of $MgH_2P_2O_7$

Atom	*x*	*Y*	*z*	$U_{iso} \times 100$
Mg1	0.242(3)	0.247(2)	0.244(4)	0.2(2)
Mg2	0.254(1)	0.4116(4)	0.002(2)	0.2(2)
P1	0.484(1)	0.288(8)	0.566(6)	0.2(2)
P2	0.461(6)	0.041(2)	0.275(4)	0.2(2)
P3	-0.003(2)	0.218(9)	-0.066(7)	0.2(2)
P4	0.022(9)	0.454(1)	0.217(1)	0.2(2)
O1	0.158(1)	0.396(1)	0.184(9)	0.2(2)

O2	0.350(9)	0.112(4)	0.319(4)	0.2(2)
O3	0.425(1)	0.329(2)	0.408(2)	0.2(2)
O4	0.069(1)	0.171(2)	0.086(9)	0.2(2)
O5	0.379(5)	0.287(4)	0.115(7)	0.2(2)
O6	-0.058(8)	0.372(4)	0.315(2)	0.2(2)
O7	0.393(4)	-0.064(3)	0.196(2)	0.2(2)
O8	0.124(9)	0.542(6)	0.316(7)	0.2(2)
O9	0.121(6)	0.220(9)	0.404(8)	0.2(2)
O10	0.115(4)	0.522(8)	-0.108(8)	0.2(2)
O11	0.519(3)	0.387(9)	0.659(5)	0.2(2)
O12	0.403(4)	0.520(6)	0.107(2)	0.2(2)
O13	0.651(6)	0.248(4)	0.602(4)	0.2(2)
O14	-0.159(1)	0.284(4)	-0.096(1)	0.2(2)

Table 8: Bond lengths for a unit cell of $MgH_2P_2O_7$

Atoms	Bond length (Å)
Mg1-O1	2.06(9)
Mg1-O2	2.00(1)
Mg1-O3	2.20(9)
Mg1-O4	2.09(9)

Mg1-O5	2.04(3)
Mg1-O9	2.14(7)
Mg2-O1	2.17(1)
Mg2-O2	2.18(4)
Mg2-O5	2.06(05)
Mg2-O9	2.12(3)
Mg2-O10	1.98(7)
Mg3-O12	1.99(9)
P1-O3	1.55(9)
P1-O5	1.51(3)
P1-O11	1.52(6)
P1-O13	1.53(8)
P2-O2	1.58(6)
P2-O7	1.58(7)
P2-O11	1.64(5)
P2-O12	1.44(3)
P3-O4	1.54(1)
P3-O6	1.60(9)
P3-P9	1.46(2)
P3-P14	1.60(6)

P4-O1	1.54(6)
P4-O6	1.70(6)
P4-O8	1.57(2)
P4-O10	1.42(6)

Table 9: Selected bond angles for the unit cell of MgH_2P_2O

Atoms	Angles (degrees)
O1-Mg1-O3	84.75(3)
O1-Mg1-O4	94.55(4)
O1-Mg1-O5	80.73(1)
O1-Mg1-O9	97.13(1)
O2-Mg1-O3	87.45(2)
O2-Mg1-O4	93.22(4)
O2-Mg1-O5	96.89(6)
O2-Mg1-O9	84.13(4)
O3-Mg1-O5	81.96(6)
O3-Mg1-O9	89.74(1)
O4-Mg1-O5	97.25(4)
O4-Mg1-O9	91.04(3)
O1-Mg2-O5	77.75(2)

O1-Mg2-O9	89.08(5)
O1-Mg2-O10	99.32(7)
O1-Mg2-O12	91.07(1)
O2-Mg2-O5	91.98(2)
O2-Mg2-O9	80.44(1)
O2-Mg2-O10	90.11(4)
O2-Mg2-O12	98.11(5)
O5-Mg2-O9	77.79(8)
O5-Mg2-O12	93.98(3)
O9-Mg2-O10	97.12(8)
O10-Mg2-O12	91.20(9)
O3-P1-O5	116.30(1)
O3-P1-O11	104.42(8)
O3-P1-O13	112.69(1)
O5-P1-O11	112.74(9)
O5-P1-O13	112.61(2)
O11-P1-O13	95.94(2)
O2-P2-O7	117.04(9)
O2-P2-O11	102.97(7)
O2-P2-O12	112.61(8)

O7-P2-O11	107.19(6)
O7-P2-O12	110.15(1)
O11-P2-O12	105.88(3)
O4-P3-O6	111.45(1)
O4-P3-O9	104.49(5)
O4-P3-O14	119.78(7)
O6-P3-O9	110.48(1)
O6-P3-O14	99.52(7)
O9-P3-O14	111.14(2)
O1-P4-O6	108.07(3)
O1_P4_O8	95.16(3)
O1_P4_O10	122.59(1)
O6_P4_O8	111.23(1)
O6_P4_O10	97.00(3)
O8_P4_O10	122.68(5)